Copy
RM L58A08

NACA RM L58A08

C-2

NACA

RESEARCH MEMORANDUM

INVESTIGATION OF A HIGH-FLOW TRANSONIC-COMPRESSOR INLET STAGE HAVING A HUB-TIP RADIUS RATIO OF 0.35

By A. Richard Felix

Langley Aeronautical Laboratory
Langley Field, Va.

NATIONAL ADVISORY COMMITTEE
FOR AERONAUTICS

WASHINGTON

March 6, 1958

NACA RM L58A08

NATIONAL ADVISORY COMMITTEE FOR AERONAUTICS

RESEARCH MEMORANDUM

INVESTIGATION OF A HIGH-FLOW TRANSONIC-COMPRESSOR INLET STAGE HAVING A HUB-TIP RADIUS RATIO OF 0.35

By A. Richard Felix

SUMMARY

High-thrust turbojet engines capable of operation at high flight speeds require a high weight flow of air per unit frontal area (specific weight flow). Therefore, a transonic-compressor inlet stage with a hub-tip radius ratio of 0.35 was designed for a specific weight flow of air of 37.5 lb/sec/sq ft.

Results for this stage, which was tested in Freon-12, indicated that at design speed the peak temperature efficiency was 0.85 at a corrected weight flow of 54.2 lb/sec of Freon and a stage total-pressure ratio of 1.29. The largest corrected weight flow measured was 59.7 lb/sec of Freon at 120 percent of design speed. This corresponds to a specific weight flow of air of 40.6 lb/sec/sq ft. Comparison of these stage tests with rotor-alone tests indicated that the addition of the stator reduced the efficiency by 3 to 5 percent without materially affecting the weight-flow range or total-pressure ratios.

The rotor blade-element data indicated high losses in the tip region, particularly at the higher speeds. Also noted was a tendency for the minimum-loss angle of attack to increase as the speed was increased.

The stator blade-element data showed reasonably low minimum losses at all blade elements. These minimum losses occurred near the design angle of attack at all blade elements except those near the ends of the blade.

INTRODUCTION

The primary requirement for high-thrust turbojet engines capable of operation at high flight speeds is a high weight flow of air per unit frontal area (specific weight flow). For a compressor with a given tip diameter, the weight flow can be increased by decreasing the hub-tip ratio

or by increasing the axial velocity, or both. If the axial Mach number of the flow entering the compressor is to be kept down to a reasonable value (0.7 or less) when the compressor is designed for specific weight flows of 35 to 38 lb/sec/sq ft, the hub-tip radius ratio must be near 0.35. These high specific weight flows in conjunction with tip speeds near 1,000 ft/sec produce Mach numbers relative to the rotor tip section that are in the transonic range (1.0 to 1.2).

As part of a program to investigate high-flow transonic compressors, a rotor with a hub-tip radius ratio of 0.35 was designed for a specific weight flow of 37.5 lb/sec/sq ft and a tip speed of 972 ft/sec. This rotor was tested in a 3,000-horsepower test rig at the Langley Laboratory and the results of these tests are reported in references 1 and 2. The purpose of the present phase of the program was to investigate the performance of a stage (rotor-stator combination). Therefore, a stator was designed and built for use with the rotor of references 1 and 2. This stator was designed to turn the flow to the axial direction.

The stage was tested in Freon-12 in the 3,000-horsepower test rig at five speeds: 80, 90, 100, 110, and 120 percent of design speed. Data presented in this report include overall performance of the stage, performance of the rotor and stator blade elements, and radial distribution of flow parameters behind the rotor and behind the stator.

SYMBOLS

A_f	frontal area, sq ft
c	blade chord, ft
C_{l_o}	camber expressed as lift coefficient of isolated airfoil
C_p	static-pressure-rise coefficient (see appendix)
c_p	specific heat at constant pressure, $ft^2/sec^2\text{-}^oR$
D	diffusion factor (see appendix)
M	Mach number
N	rotor speed, rpm
P	total pressure, lb/sq ft

P_f	total pressure at station 3 outside stator wake
p	static pressure, lb/sq ft
r	radius, ft
T	total temperature, ^{o}R
t	maximum thickness of blade, ft
U	rotational velocity, ft/sec
V	gas velocity, ft/sec
w	weight flow, lb/sec
w_e	corrected weight flow, $w\frac{\sqrt{\theta}}{\delta}$, lb/sec
α	angle of attack (angle between relative flow direction and chord line), deg
β	flow angle, measured from axial direction, deg
δ	ratio of inlet total pressure to NACA standard sea-level pressure of 2,116.22 lb/sq ft
η_T	temperature-rise efficiency
γ	ratio of specific heats
ρ	mass density, slugs/cu ft
σ	solidity (ratio of blade chord to circumferential blade spacing)
θ	ratio of inlet total temperature to NACA standard sea-level temperature of 518.688^{o} R
θ_o	flow turning angle, deg
$\bar{\omega}$	total-pressure-loss coefficient

Subscripts:

A	air
av	average

[redacted]

d	design
F	Freon-12
h	hub
i	ideal
m	mean section
R	relative to rotor blades
S	stator
t	tip
z	axial
θ	tangential
1	upstream of rotor (station 1)
2	downstream of rotor (station 2)
3	downstream of stator (station 3)

Figure 1 shows a typical velocity diagram.

APPARATUS AND PROCEDURE

Rotor Design

The rotor design is described in detail in reference 1. The design weight flow in air is 37.5 lb/sec/sq ft and the design total-pressure ratio varies from 1.25 at the hub to 1.35 at the tip. Moderate rather than high pressure ratios were used in this design since the main purpose was to obtain a high specific weight flow. The design velocity diagrams were obtained by satisfying simple radial equilibrium $\left(\frac{dp}{dr} = \frac{\rho V_\theta^2}{r}\right)$ in the rotor calculation. A typical velocity diagram is shown in figure 1. The rotor blade sections chosen to fulfill the design velocity diagrams made use of an A_{10}, or constant-loading, mean line at the hub section and the loaded-trailing-edge mean lines A_6I_{4b} and A_2I_{8b} at the mean and tip sections, respectively. (See ref. 3 for explanation of designations.) The maximum

[redacted]

thickness was at the 65-percent-chord point for all sections (ref. 1). A photograph of the rotor is shown in figure 2. Table I presents the rotor blade-section data.

Because of a bearing failure and subsequent blade damage, it was not possible to use the original rotor, the test results for which were reported in references 1 and 2, in making the stage tests reported herein. A duplicate rotor was built especially for this test program. A check of the blade-setting angles of this duplicate rotor revealed that the blades were set at 1° too small an angle with reference to the axial direction at all blade elements. This means that at a given speed and weight flow, each blade element was operating at a 1° higher angle of attack than the proper blade-setting angle would have produced. This error affects the overall performance of the rotor, and consequently the stage, and will be discussed in the section on "Overall Performance."

Stator Design

The stator for this stage was designed to turn the rotor outlet flow to the axial direction. The design made use of measured outlet flow conditions available from the rotor tests reported in reference 2. The blade sections used were NACA 65-series with constant loading (A_{10}) mean lines. References 4 and 5 were used in the blade-section selection. Thickness-chord ratios of 0.08 were used at all elements. The chord length varied from 2.505 inches at the hub to 3.425 inches at the tip. Eleven blades were used, and the solidity varied from 1.500 at the hub to 1.000 at the tip. A photograph of the stator with the outer and inner casing is shown as figure 3. The stator blade-section data are summarized in table I. The stator turning angles and inlet-flow angles used in obtaining the section cambers were based upon inlet conditions and uncorrected for axial-velocity change through the stator. If the choice of blade section had been based on mean-axial-velocity diagrams, a lower camber would have been used at the tip section and a slightly higher camber would have been required at the hub section.

Installation

The stage tests reported herein were made in the 3,000-horsepower test rig which is described in references 1 and 6. A schematic diagram of the closed system is presented in figure 4. Freon-12 was used as a test medium in order to achieve a higher Mach number level for a given rotor speed. The tip diameter of this stage was 12 inches. A layout of the test section is shown in figure 5.

Procedure and Test Conditions

Stage tests were made for a range of corrected tip speeds from 80 to 120 percent of design speed. At each speed, the weight flow was varied from the maximum to the surge point by continuously increasing the back pressure. Five weight-flow points or throttle settings were used at each speed. The settling-chamber pressure was held constant at approximately 20 inches of mercury absolute, and the settling-chamber temperature was fixed at values between 55° F and 85° F.

Instrumentation

Flow conditions were measured at three axial locations: station 1, approximately 1.5 inches upstream of the rotor leading edge; station 2, approximately 0.25 inch downstream of the rotor trailing edge; and station 3, approximately 0.5 inch downstream of the stator trailing edge. (See fig. 5.)

Total pressures and total temperatures of the Freon entering the rotor were obtained from pressure orifices and temperature rakes in the settling chamber. Static pressure of the Freon entering the rotor was measured by four static-pressure orifices on the inner casing and four on the outer, spaced at 90° circumferential intervals at station 1.

Total pressure, static pressure, and flow angle were measured at 10 equal-area centers at station 2 by traversing the passage radially with a prism-type probe (ref. 7). Static pressures were also measured by eight static-pressure orifices located on the inner and outer casing in the same manner as those at station 1. Total temperatures were obtained at station 2 by means of two five-bell chromel-alumel thermocouple rakes spaced radially to cover the entire passage. These rakes were connected to a single five-bell chromel-alumel rake at station 1 to give the temperature differential across the rotor. The prism-type survey probe and one of the chromel-alumel thermocouple rakes are shown in figure 6.

Downstream of the stator, at station 3, the total pressure, static pressure, and flow angle were measured by traversing the annulus with a prism-type probe as was done at station 2. Wall static-pressure orifices were also used as at stations 1 and 2. Two five-bell chromel-alumel thermocouple rakes at station 3 were used in conjunction with the five-bell rake at station 1 to measure the stage temperature rise at 10 radial locations. The total-pressure loss in the stator wake was obtained through the use of a 17-tube circumferential total-pressure rake. This rake moved radially and covered approximately one-half of the blade spacing at the tip and one blade spacing at the hub. A photograph of the rake is included in figure 6. These wake measurements were made at five radial locations.

Accuracy

Since the integrated weight flows at stations 2 and 3 make use of three of the measured flow properties - absolute flow angle, static pressure, and total pressure - it is believed that a comparison of these weight flows with those measured by a calibrated venturi gives a reasonable indication of the accuracy of the measurements at stations 2 and 3. The weight flows agreed with the venturi meter values within 4 percent, and are considered acceptable. As a further check on accuracy, the temperature and momentum efficiencies were compared and found to agree within 3 percent, which is also considered quite acceptable.

RESULTS AND DISCUSSION

Overall Performance

The overall pressure ratios and temperature efficiencies presented for the stage are mass-weighted averages. The equations used are given in the appendix. It should be pointed out that the use of 10 equal-area centers in the mass weighting of overall efficiencies and pressure ratios includes some of the boundary-layer influence.

Temperature efficiencies rather than momentum efficiencies are presented in this paper, since the difficulties encountered in making temperature measurements for the rotor-alone tests of reference 1 have been overcome. The measured momentum and temperature efficiencies of these stage tests generally agreed within 3 percent, the momentum efficiency being the higher.

Figure 7 is a plot of overall pressure ratio and temperature efficiency of the stage as functions of corrected weight flow of Freon at the five corrected speeds, 80, 90, 100, 110, and 120 percent of design speed. The specific weight flows of air which correspond to the inlet axial Mach numbers obtained in Freon are also indicated (see appendix). The peak efficiency of the stage at design speed is 0.85, and it occurs at a corrected weight flow of 54.2 lb/sec of Freon and a total-pressure ratio of 1.29. The corresponding specific weight flow of air is 37.1 lb/sec/sq ft, which is very near the design value of 37.5. The peak efficiency then decreases to 0.81 for 56.1 lb/sec of Freon at 110 percent of design speed and further to 0.78 for 57.2 lb/sec of Freon at 120 percent of design speed. The total-pressure ratio for peak efficiency at 120 percent of design speed is 1.42. The largest weight flow of the tests is 59.7 lb/sec of Freon at the 120-percent speed. This corresponds to a specific weight flow of air of 40.6 lb/sec/sq ft. At 80 and 90 percent of design speed, the peak efficiencies are 0.82.

[redacted]

At these speeds the stage exhibited a wide range of efficient weight flow (20 percent or more) which holds up reasonably well at the higher speeds. Only the 120-percent speed data showed as much as an 8-percent difference between the highest and lowest efficiency measured.

The construction error in the rotor blade-setting angles makes it difficult to compare these stage tests with the rotor-alone tests of reference 1. However, a rough comparison seems to indicate that the addition of the stator did not materially affect the weight-flow range or the total-pressure ratios. A comparison of the stage and rotor-alone momentum efficiencies showed the stage values to be 3 to 5 percent lower. Most of this drop can be attributed to the losses through the stator.

The fact that, at the higher speeds, the weight flows passed by the stage were higher than those passed by the rotor alone is not the result of the addition of the stator but the result of the error in blade-setting angle. Since the rotor surge point, or minimum weight flow, is in effect a stall at positive angle of attack, the lower blade-setting angles of the stage rotor cause the stalling angle of attack to occur at higher weight flows. In these tests, the maximum weight flow which can be passed at any speed is controlled by the operating requirements of the closed-loop system. Since, at a given weight flow, the rotor used in the stage tests is operating at higher angles of attack than the rotor of reference 1, it also produces a higher pressure ratio. It follows, then, that the curves for the variation of rotor pressure ratio with weight flow intersect the loop-limiting curve at higher weight flows, and thus make possible a higher maximum weight flow at each speed. It can be concluded, therefore, that the general shift of the weight-flow level in the stage tests was caused by the error in blade-setting angle.

Blade-Element Performance

Description of a blade element.- The annuli at stations 1, 2, and 3 were each divided into 10 equal concentric areas. Each of these 10 equal areas was then divided into two equal concentric areas by an "equal-area center." Blade elements, as used in this paper, are those sections of the blades which lie on conical surfaces connecting corresponding equal area centers between stations 1 and 2 for the rotor and between stations 2 and 3 for the stator. The blade-element performance was computed for all 10 blade elements in each blade row, but data for only five blade elements from each row are presented herein. The following table gives the radii of the 10 equal-area centers calculated at each of the three stations and the designations of the blade elements for which performance data are presented:

Equal-area center	Radius, ft, at -			Blade-element designation
	Station 1	Station 2	Station 3	
1	0.489	0.490	0.491	
2	.466	.469	.472	e
3	.442	.448	.453	
4	.416	.425	.432	d
5	.389	.401	.411	
6	.360	.376	.388	c
7	.328	.349	.364	
8	.292	.319	.338	b
9	.252	.286	.310	
10	.204	.249	.279	a

Rotor blade-element performance.- Figure 8 presents the rotor blade-element performance as a function of angle of attack.

At elements b and c, the minimum relative total-pressure-loss coefficient $\overline{\omega}_R$ is 0.1 or less for all speeds tested. The scatter in the loss data at element a is greater than that at elements b and c, but generally the minimum $\overline{\omega}_R$ is 0.12 or less. At elements d and e, the minimum-loss values begin to increase, especially at the higher speeds. At element d, the minimum $\overline{\omega}_R$ at 120 percent of design speed is about 0.15, and at element e, the minimum values are 0.14 at 90 percent speed, 0.18 at 100 percent speed, 0.23 at 110 percent speed, and 0.35 at 120 percent speed. These high losses near the tip at the higher speeds were also in evidence in the rotor-alone tests of reference 2 and are due to the combined influence of three-dimensional-flow effects, compressibility effects, and shock losses. The inlet relative Mach numbers associated with these losses at element e are as high as 1.2. A discussion of the influence of shock losses at these Mach numbers is given in reference 8. The design angle of attack is indicated by arrows at the bottom of each part of the figure. Although the rig operating limitations and the construction error in the rotor blade-setting angle prevented the attainment of design angles of attack, it appears that at the lowest speed tested, 80 percent of design, the minimum loss would have occurred near the design angle of attack at all blade elements. However, the minimum-loss angle of attack increases as the speed (inlet relative Mach number) increases. At element e, the α for minimum loss appears to increase by about 5° as the rotor speed is increased from 80 to 120 percent of design. Near the hub at element a, this trend is less pronounced, the change being about 3°. The increase near the tip is probably the result of the shock wave from one blade influencing the flow field immediately ahead of the next blade, but the reason for the increase near the hub is not clear. Similar results have been noted for transonic rotors with circular-arc blades (ref. 9). Therefore, it would seem that the trend of increasing minimum-loss α with speed might be expected with other types of blades.

[redacted]

A small amount of extrapolation of the turning-angle curves indicates excessive turning at the design angle of attack at all blade elements except element a, near the hub. The excess at elements b and e is about 4° and at elements c and d, about 6°. At element a, a slight deficiency in turning (about 1.5°) is noted. It is believed that the excessive turning in evidence over most of the blade span is caused primarily by the proximity of measuring station 2 to the rotor blades (0.25 inch). As has been noted previously (ref. 9), total pressures measured very near a rotating blade row are higher than those measured 1 to $1\frac{1}{2}$ chord lengths downstream. The fact that a total-pressure tube tends to read high in a turbulent flow field is also pointed out in appendix B of reference 10. The higher total pressure indicates a higher velocity downstream of the rotor, which in turn produces a higher turning angle.

It is believed that the magnitude of the total-pressure error is about 3 percent. Of course, any error in the measurement of the total pressures behind the rotor produces errors in other rotor blade-element parameters, but such errors should be 6 percent or less in most cases. Therefore, the primary information to be gleaned from the rotor blade-element plots is in the nature of trends and differences rather than absolute values.

The peak values of blade-element efficiency are 0.88 or more at all speeds at elements b and c. As in the case of the loss values, the scatter at element a is such that the values of peak efficiency are difficult to estimate. At element d the peak efficiency is 0.88 or more at all speeds except 120 percent of design, at which speed the peak value has dropped to 0.84. The peak efficiency at element e is 0.86 or less at all five rotor speeds.

The plots of axial velocity ratio indicate no major flow shifts with angle of attack at the three higher speeds, 100, 110, and 120 percent of design. At 80 and 90 percent of design speed, the negative slope of the curve of axial velocity ratio at element e, coupled with positive slopes at the other four elements, indicates increasing separation and an inward shift of the flow (from the tip toward the hub) as the angle of attack is increased.

The blade-loading characteristics are indicated by the diffusion factor D_R and the static-pressure-rise coefficient $C_{p,R}$. The values of D_R were 0.6 or less at all blade elements except the tipmost element e. At this element, values of D_R as high as 0.75 and relative total-pressure-loss coefficients as high as 0.46 were measured. The peak static-pressure-rise coefficients generally increased with speed until they reached a maximum at 100 or 110 percent of design speed and then

decreased slightly at 120 percent of design speed. This decrease can be attributed to the larger total-pressure-loss coefficients at 120 percent of design speed. The peak $C_{p,R}$ value measured at elements a, b, and c varied from 0.52 to 0.58. At element d the peak value was 0.45 and at element e, 0.40. Thus, at element e the high losses due to separation affect the two loading parameters oppositely, causing generally greater D_R values than at the other blade elements, and smaller $C_{p,R}$ values.

Radial distribution of parameters at rotor outlet.- In figure 9 are presented the radial variation of rotor-outlet absolute flow angle β_2, rotor total-pressure ratio P_2/P_1, rotor element efficiency η_T, and rotor-outlet absolute Mach number M_2. Data are presented for three operating points at each of the five speeds of the investigation. The three points correspond to (1) the maximum weight flow, (2) the weight flow for maximum overall efficiency, and (3) the near-surge weight flow. (An exception was made at 100 percent of design speed. Since the maximum-efficiency point corresponded with the maximum-weight-flow point, an intermediate weight-flow point was included in order to present a more complete picture.)

The curves for absolute flow angle at station 2 plotted against radius have substantially the same slope throughout the range of weight flows and speeds, if the high-loss tip region is neglected. It can be seen in figure 9(a) that although the slopes of the β_2 curves are similar, the level increases as the weight flow decreases. This change at a given speed is primarily the result of the decreased axial velocity at the lower weight flows. A comparison of figure 9(a) with figure 9(e) shows that the β_2 level also increases with speed. The general drop in the axial velocity ratio $V_{z,2}/V_{z,1}$ as the speed is increased is the main cause for this increase in β_2. The absolute Mach number at station 2 for each speed and weight flow is fairly constant radially except near the tip. The average values of M_2 for the maximum flow condition at 80, 100, and 120 percent of design speed are 0.60, 0.71, and 0.86, respectively.

At each of the speeds, with the weight flow for maximum overall efficiency, the blade-element effiency is reasonably constant and high over the middle portion of the blade, but drops considerably at the tip and, to a lesser extent, at the hub. It is to be noted that the low overall efficiency with the highest weight flow at 110 and 120 percent of design speed is due to the drop in element efficiency in the tip region. For the highest weight flow, at 120 percent of design speed, the lower efficiency extends inboard to the middle of the blades. These lower efficiency values are also reflected by the dropoff in total-pressure ratios over the outer half of the blade.

[redacted]

Stator blade-element performance.- Figure 10 presents the stator blade-element performance as a function of angle of attack α_S. Before discussing the stator blade-element plots, it is desirable to describe the stator total-pressure-loss coefficient $\bar{\omega}_S$. This coefficient is defined as the difference between the stator-outlet total pressure outside the wake P_f and the average total pressure at station 3 divided by the difference between the total pressure at station 2 and the static pressure at station 2. Figure 11 presents typical plots of the circumferential distribution of total pressure at two radial locations at station 3. The symbol P_f denotes an area average of the total pressures across one blade passage excluding the blade wake (indicated in figure 11 by a long-dash line). The average total pressure at station 3 is an area average of the total pressure across one blade passage including the blade wake (indicated in figure 11 by a short-dash line). At the higher speeds, the stator total-pressure-loss coefficients are not as reliable as at the lower speeds because of the difficulty in determining the magnitude of P_f. This difficulty is caused by the fact that the total pressure outside the stator wake is very uneven at the higher speeds and consequently the proper level of the area average is difficult to determine. This is particularly true near the hub.

The lowest total-pressure-loss coefficient in figure 10 is 0.07 or less at all five of the blade elements. At elements b, c, and d, the minimum loss occurs near (within 2° of) the design angle of attack. The fact that the measured angles of attack are all above design, at the three higher speeds, is caused primarily by the lower axial velocity ratios across the rotor at the three higher speeds. The minimum loss near the blade ends, elements a and e, occurs several degrees above the design angle of attack. Near the blade tip, element e, this characteristic may be due to the radial inflow of the blade boundary layer. At element a, however, this trend of decreasing loss with increasing angle of attack is more difficult to explain. It may possibly be due to the difficulty, mentioned previously, in determining P_f.

The stator turning angles are nearly linear in their variation with angle of attack even in the high-loss regions at elements b, c, d, and e. The design turning angles are indicated by the solid symbols, and the off-design turning-angle characteristics as obtained from the low-speed cascade data of reference 4 are indicated by the dashed lines. At elements b, c, d, and e, the slopes of the turning-angle curves are very similar to those from the low-speed cascade data. At element b, design turning was measured at design angle of attack. The turning measured at the design angle of attack at elements c, d, and e, was excessive by 1.2°, 3.6°, and 6.2°, respectively. At the blade element nearest the hub, element a, the linear relationship of the turning angle with angle of attack breaks down, although at the three higher speeds, 100, 110, and

120 percent of design, the measured turning angles at the lower angles of attack are near design. As was mentioned in the section entitled "Stator Design," the stator design turning angles and inlet angles were not corrected for axial-velocity variation before the cambers and blade-setting angles were chosen. Since the design axial-velocity ratios were greater than 1 in the tip region and slightly less than 1 in the hub region, this correction would have resulted in the use of lower cambers near the tip and slightly higher cambers near the hub. This, in turn, would have reduced or eliminated the excessive turning at elements c, d, and e. Also, the use of lower cambers at lower angles of attack would very likely reduce the stator losses. It is believed that the excessive turning at the stator is not the result of an error in the total-pressure measurement, as was the case in the rotor turning angles, because station 3 is far enough downstream of the rotor to allow mixing to take place.

The values of D_S were generally found to be 0.6 or less at all blade elements, as was noted for most of the rotor elements. At elements b, c, and d, the values of D_S for minimum loss were in the range from 0.3 to 0.4, whereas, near the blade ends at elements a and e, the values of D_S for minimum loss were somewhat higher, particularly at element a. The maximum static-pressure-rise coefficients increased from about 0.2 at element e to about 0.55 at element a. The values of $C_{p,S}$ for minimum loss were in the range from 0.05 to 0.20 for elements b, c, d, and e, and near 0.5 for element a. The low level of the static-pressure-rise coefficients measured at the outer blade elements can be attributed to axial-velocity ratios greater than 1 and to turning past the axial direction.

Radial distribution of parameters at the stator outlet.- Figure 12 presents the radial variation of stator outlet flow angle β_3 and stator outlet Mach number M_3. These plots are presented in the same manner as the rotor outlet plots, and the same weight flows are used.

Since the stator was designed to turn the rotor outlet flow to the axial direction, the optimum value of β_3 would be zero at all radii. The sign convention for the plots of β_3 is such that a positive angle indicates deficient turning and a negative angle excess turning. The radial plots of β_3 do not appear to change significantly with speed, either in shape or level. For all weight flows, the values of β_3 were negative over the outboard half of the blade, the lowest values being near -12°. For the highest weight flow at each speed, the values of β_3 were near zero over the inboard half of the blade. At the lower two weight flows at each speed, the values of β_3 became positive near the hub, indicating deficient turning due to the breakdown in the linear relationship between turning angle and angle of attack mentioned in the previous section. The excessive turning over the outer half of the stator

blades was the result of the use of too high a camber and possibly some boundary-layer inflow.

The variation of the stator outlet Mach number M_3 with radius is fairly linear except near the blade ends. The increase in slope with speed is due to compressibility effects. For a given speed and weight flow, the average Mach number of the flow leaving the stator is roughly the same as the absolute Mach number of the gas entering the rotor.

Figure 13 presents the radial distribution of weight-flow ratio at station 1, station 2, and station 3 for three weight flows at design speed. The three weight flows presented are (1) the maximum weight flow, 54.2 lb/sec, (2) an intermediate weight flow, 51.9 lb/sec, and (3) the near-surge weight flow, 49.1 lb/sec. The weight flow is presented as a nondimensional parameter $\rho V_z/(\rho V_z)_{1,m}$, where the subscript 1,m indicates the mean section (at a radius of 0.360 foot) at station 1. As the weight flow is increased, the radial distribution remains substantially unchanged, the only noticeable characteristic being a slight outward shift at station 2. At design speed, the average flow blockage factor was 0.96 at station 2 and 0.95 at station 3. The blockage factor is defined as the ratio of the integrated mass flow to the integrated mass flow when extrapolated to the walls. This extrapolation merely excludes the effect of the wall boundary layer. The blockage factor behind the stator also includes the effect of wake blockage.

SUMMARY OF RESULTS

Tests of a high-flow transonic inlet stage gave the results summarized in the following sections.

Rotor Blade-Element Performance

1. Reasonably good peak efficiency (0.85 or more) was measured at all elements at speeds up to design, except at the outermost blade element (about 11 percent of the blade span from the outer casing).

2. High total-pressure losses were measured in the tip region, particularly at the higher speeds; these high losses were also in evidence in the rotor-alone tests previously reported.

3. As the speed was increased from 80 to 120 percent of design, the minimum-loss angle of attack near the tip increased by about 5°. Near the hub the increase was slightly less, being about 3°.

Stator Blade-Element Performance

1. The lowest total-pressure-loss coefficient is about 0.07 or less at all the blade elements for which results are presented.

2. The minimum loss occurs near the design angle of attack at all elements except near the blade ends.

3. Excessive turning occurred at all speeds over the outer half of the blade, as compared with design values.

Overall Stage Performance

1. At design speed, the peak stage efficiency was 0.85 at a corrected weight flow of 54.2 lb/sec of Freon and a stage total-pressure ratio of 1.29. The corresponding specific weight flow of air is 37.1 lb/sec/sq ft, which is very near the design value of 37.5.

2. At 120 percent of design speed the peak efficiency is 0.78 at 57.2 lb/sec and a total-pressure ratio of 1.42.

3. The largest corrected weight flow measured at 120 percent of design speed is 59.7 lb/sec of Freon. This is equal to a specific weight flow for air of 40.6 lb/sec/sq ft.

4. The weight-flow range is about 20 percent or more at the lower speeds and holds up reasonably well even at 100 and 120 percent of design speed. Only the highest speed had as much as an 8-percent drop between the highest and lowest values of efficiency measured.

5. Comparison with rotor-alone tests previously reported indicated that the addition of the stator did not materially affect the weight-flow range or total-pressure ratios, although it did decrease the values of efficiency by 3 to 5 percent.

Langley Aeronautical Laboratory,
National Advisory Committee for Aeronautics,
Langley Field, Va., December 18, 1957.

[redacted]

APPENDIX

EQUATIONS

Rotor

Blade-element temperature-rise efficiency:

$$\eta_T = \frac{T_1\left[\left(\frac{P_2}{P_1}\right)^{\frac{\gamma-1}{\gamma}} - 1\right]}{T_2 - T_1}$$

Blade-element relative total-pressure-loss coefficient:

$$\bar{\omega}_R = \frac{P_{2,R,i} - P_{2,R}}{P_{1,R} - p_1}$$

$$= \frac{\left(\frac{P_{2,R}}{P_{1,R}}\right)_i - \frac{P_{2,R}}{P_{1,R}}}{1 - \frac{p_1}{P_{1,R}}}$$

where

$$\left(\frac{P_{2,R}}{P_{1,R}}\right)_i = \left(\frac{T_{1,R} + \frac{U_2^2 - U_1^2}{2c_p}}{T_{1,R}}\right)^{\frac{\gamma}{\gamma-1}}$$

Blade-element diffusion factor:

$$D_R = 1 - \frac{V_{2,R}}{V_{1,R}} + \frac{V_{\theta,1,R} - V_{\theta,2,R}}{2\sigma V_{1,R}}$$

Blade-element static-pressure-rise coefficient:

$$C_{p,R} = \frac{p_2 - p_1}{P_{1,R} - p_1}$$

Stator

Blade-element total-pressure-loss coefficient:

$$\bar{\omega}_S = \frac{P_f - P_{3,av}}{P_2 - p_2}$$

Blade-element diffusion factor:

$$D_S = 1 - \frac{V_3}{V} + \frac{V_{\theta,2} - V_{\theta,3}}{2\sigma V_2}$$

Blade-element static-pressure-rise coefficient:

$$C_{p,S} = \frac{p_3 - p_2}{P_2 - p_2}$$

Stage

Mass-averaged temperature-rise efficiency:

$$\bar{\eta}_T = \frac{T_1 \int_{r_{3,h}}^{r_{3,t}} \left[\left(\frac{P_3}{P_1} \right)^{\frac{\gamma-1}{\gamma}} - 1 \right] \rho_3 V_{z,3} r_3 \, dr_3}{\int_{r_{3,h}}^{r_{3,t}} (T_3 - T_1) \rho_3 V_{z,3} r_3 \, dr_3}$$

Mass-averaged total-pressure ratio:

$$\frac{P_3}{P_1} = \frac{\int_{r_{3,h}}^{r_{3,t}} \left(\frac{P_3}{P_1}\right) \rho_3 V_{z,3} r_3 \, dr_3}{\int_{r_{3,h}}^{r_{3,t}} \rho_3 V_{z,3} r_3 \, dr_3}$$

Conversion of Freon Weight Flow to Air Weight Flow

$$w_{e,A} = w_{e,F} \sqrt{\frac{\gamma_A R_F}{\gamma_F R_A}} \frac{\left(1 + \frac{\gamma_F - 1}{2} M^2\right)^{\frac{\gamma_F + 1}{2(\gamma_F - 1)}}}{\left(1 + \frac{\gamma_A - 1}{2} M^2\right)^{\frac{\gamma_A + 1}{2(\gamma_A - 1)}}}$$

[redacted]

REFERENCES

1. Savage, Melvyn, and Felix, A. Richard: Investigation of a High-Performance Axial-Flow Compressor Transonic Inlet Rotor Designed for 37.5 Pounds Per Second Per Square Foot of Frontal Area - Aerodynamic Design and Overall Performance. NACA RM L55A05, 1955.

2. Felix, A. Richard, and Savage, Melvyn: Investigation of a High-Performance Axial-Flow Compressor Transonic Inlet Rotor Designed for 37.5 Pounds Per Second Per Square Foot of Frontal Area - Detailed Blade-Element Performance. NACA RM L56K23, 1956.

3. Erwin, John R., Savage, Melvyn, and Emery, James C.: Two-Dimensional Low-Speed Cascade Investigation of NACA Compressor Blade Sections Having a Systematic Variation in Mean-Line Loading. NACA TN 3817, 1956. (Supersedes NACA RM L53I30b.)

4. Felix, A. Richard: Summary of 65-Series Compressor-Blade Low-Speed Cascade Data by Use of the Carpet-Plotting Technique. NACA TN 3913, 1957. (Supersedes NACA RM L54H18a.)

5. Herrig, L. Joseph, Emery, James C., and Erwin, John R.: Effect of Section Thickness and Trailing-Edge Radius on the Performance of NACA 65-Series Compressor Blades in Cascade at Low Speeds. NACA RM L51J16, 1951.

6. Goldberg, Theodore J., Boxer, Emanuel, and Bernot, Peter T.: Experimental Investigation of an Axial-Flow Supersonic Compressor Having Rounded Leading-Edge Blades With an 8-Percent Mean Thickness-Chord Ratio. NACA RM L53G16, 1953.

7. Schulze, Wallace M., Ashby, George C., Jr., and Erwin, John R.: Several Combination Probes for Surveying Static and Total Pressure and Flow Direction. NACA TN 2830, 1952.

8. Schwenk, Francis C., Lewis, George W., and Hartmann, Melvin J.: A Preliminary Analysis of the Magnitude of Shock Losses in Transonic Compressors. NACA RM E57A30, 1957.

9. Montgomery, John C., and Glaser, Frederick W.: Experimental Investigation of a 0.4 Hub-Tip Diameter Ratio Axial-Flow Compressor Inlet Stage at Transonic Inlet Relative Mach Numbers. II - Stage and Blade-Element Performance. NACA RM E54I29, 1955.

10. Davis, Wallace F., and Scherrer, Richard: Aerodynamic Principles for the Design of Jet-Engine Induction Systems. NACA RM A55F16, 1956.

[redacted]

TABLE I.- DESIGN VALUES AND GEOMETRY

(a) Rotor blade

r_1/r_t	r_2/r_t	$\beta_{1,R}$, deg	$\theta_{o,R}$, deg	C_{l_o}	σ	t/c	α, deg
0.350	0.450	27.7	35.4	1.55	1.500	0.080	21.0
.585	.646	41.3	22.3	1.14	1.063	.060	14.6
.750	.787	48.1	16.0	.89	.900	.050	11.5
.883	.902	52.3	12.9	.77	.809	.043	9.9
1.000	1.000	55.3	11.3	.70	.750	.040	8.9

(b) Stator blade

r_1/r_t	r_2/r_t	$\beta_2 = \theta_{o,S}$, deg	C_{l_o}	σ	t/c	α, deg
0.450	0.525	38.0	1.87	1.500	0.08	16.6
.646	.676	33.9	1.78	1.331	.08	14.7
.787	.799	31.4	1.74	1.203	.08	13.7
.902	.905	29.7	1.73	1.095	.08	13.2
1.000	1.000	29.0	1.73	1.000	.08	12.7

[redacted]

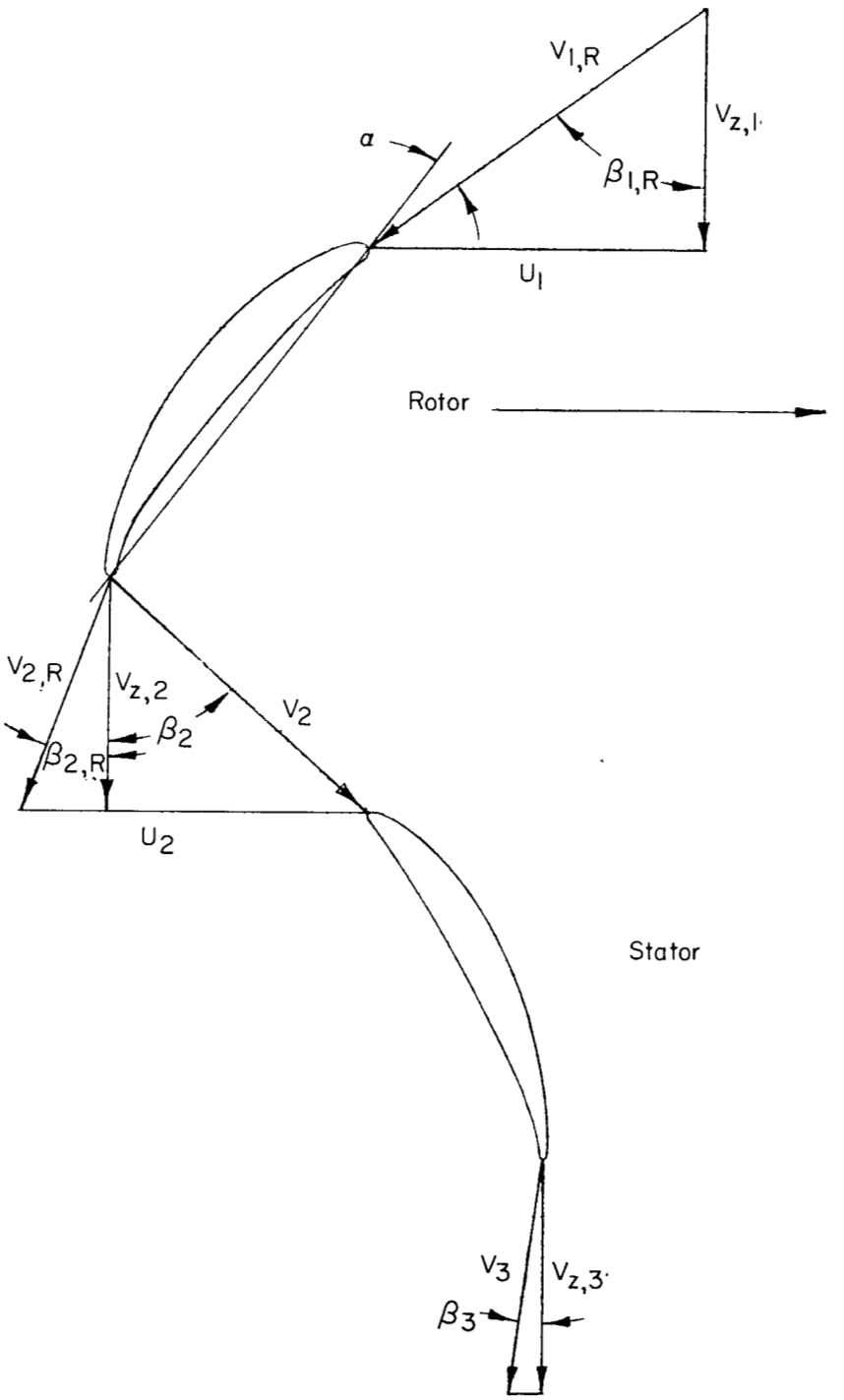

Figure 1.- Typical velocity diagrams.

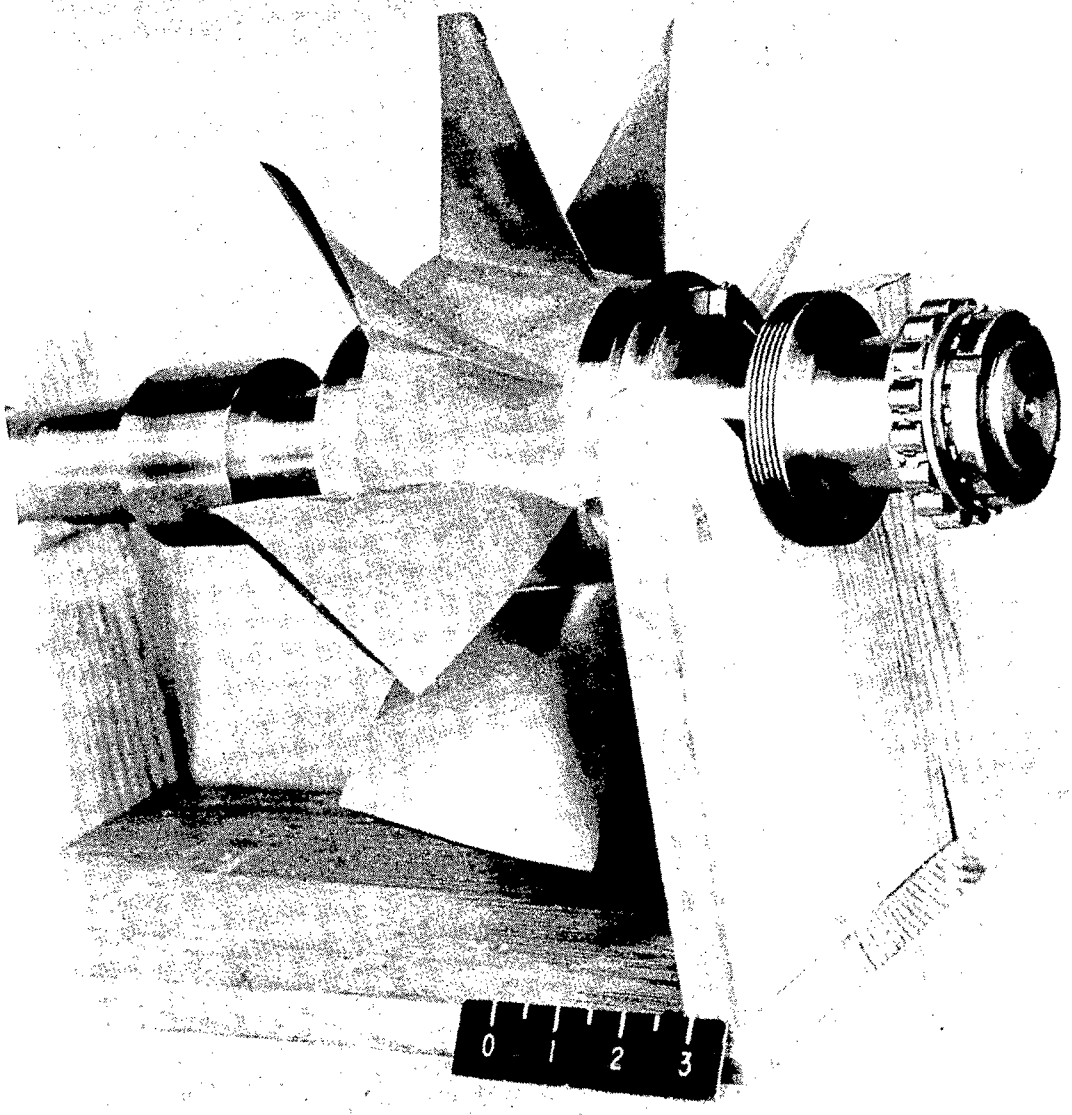

L-83845

Figure 2.- Photograph of rotor.

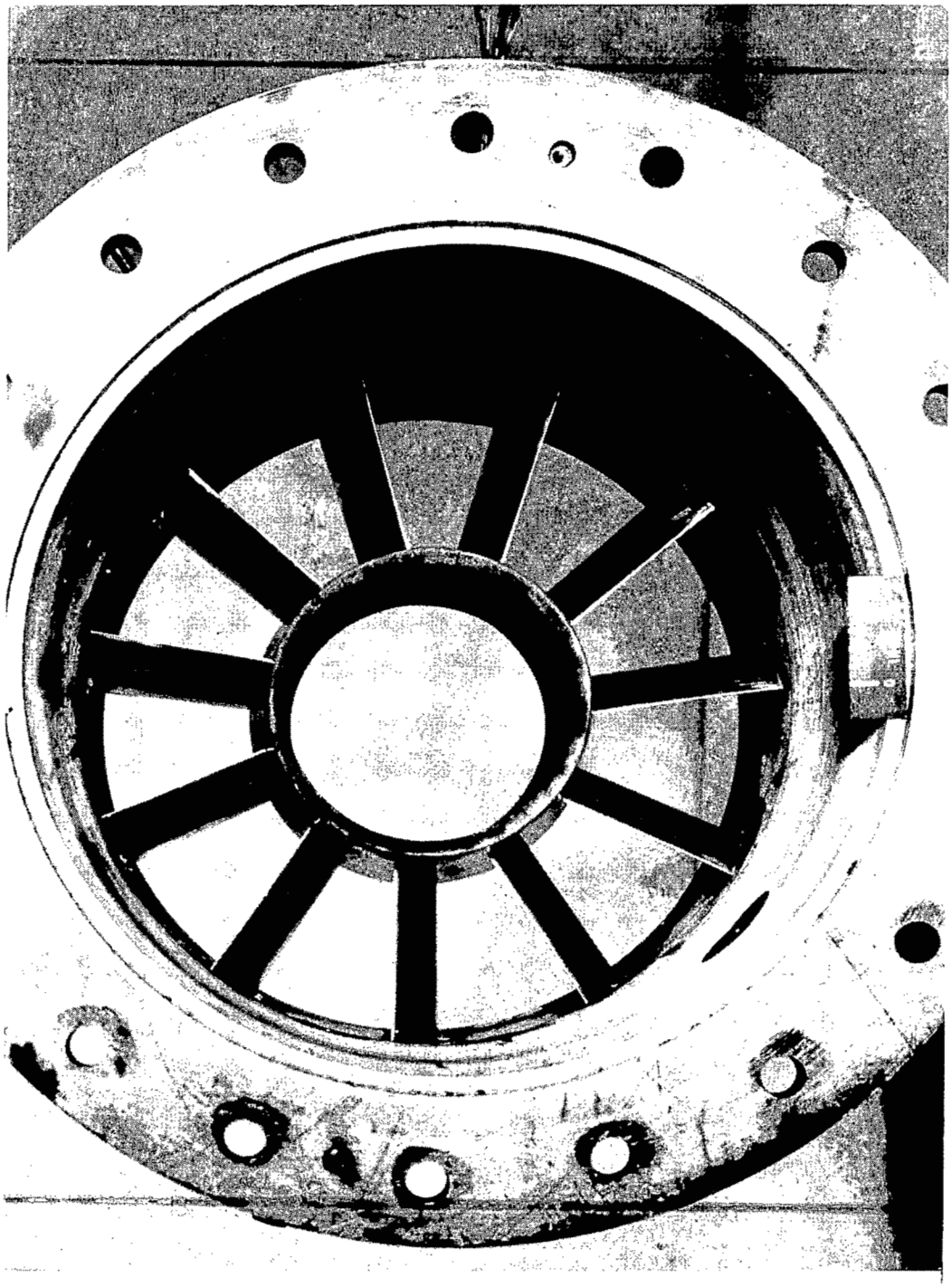

L-97004

Figure 3.- Photograph of stator.

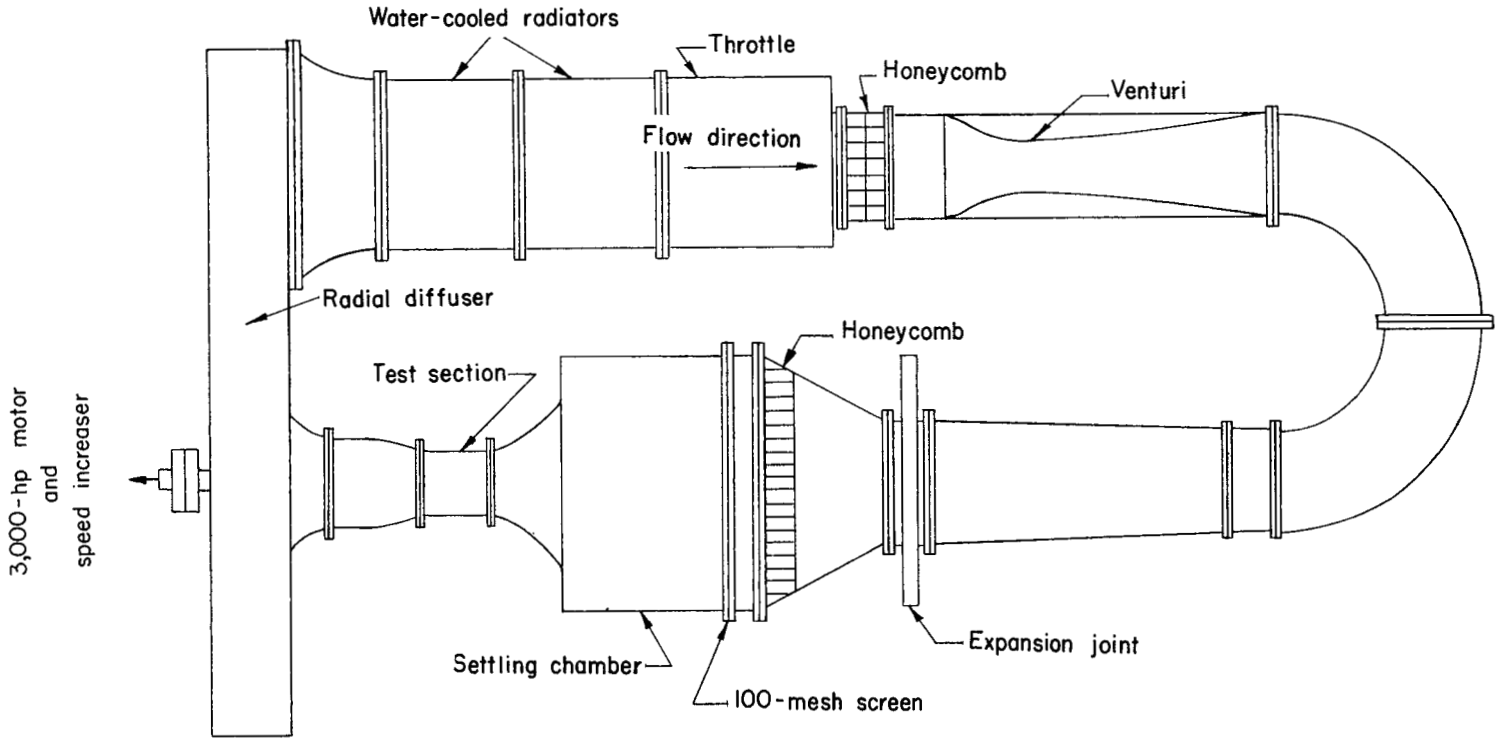

Figure 4.- Schematic diagram of 3,000-horsepower compressor test rig.

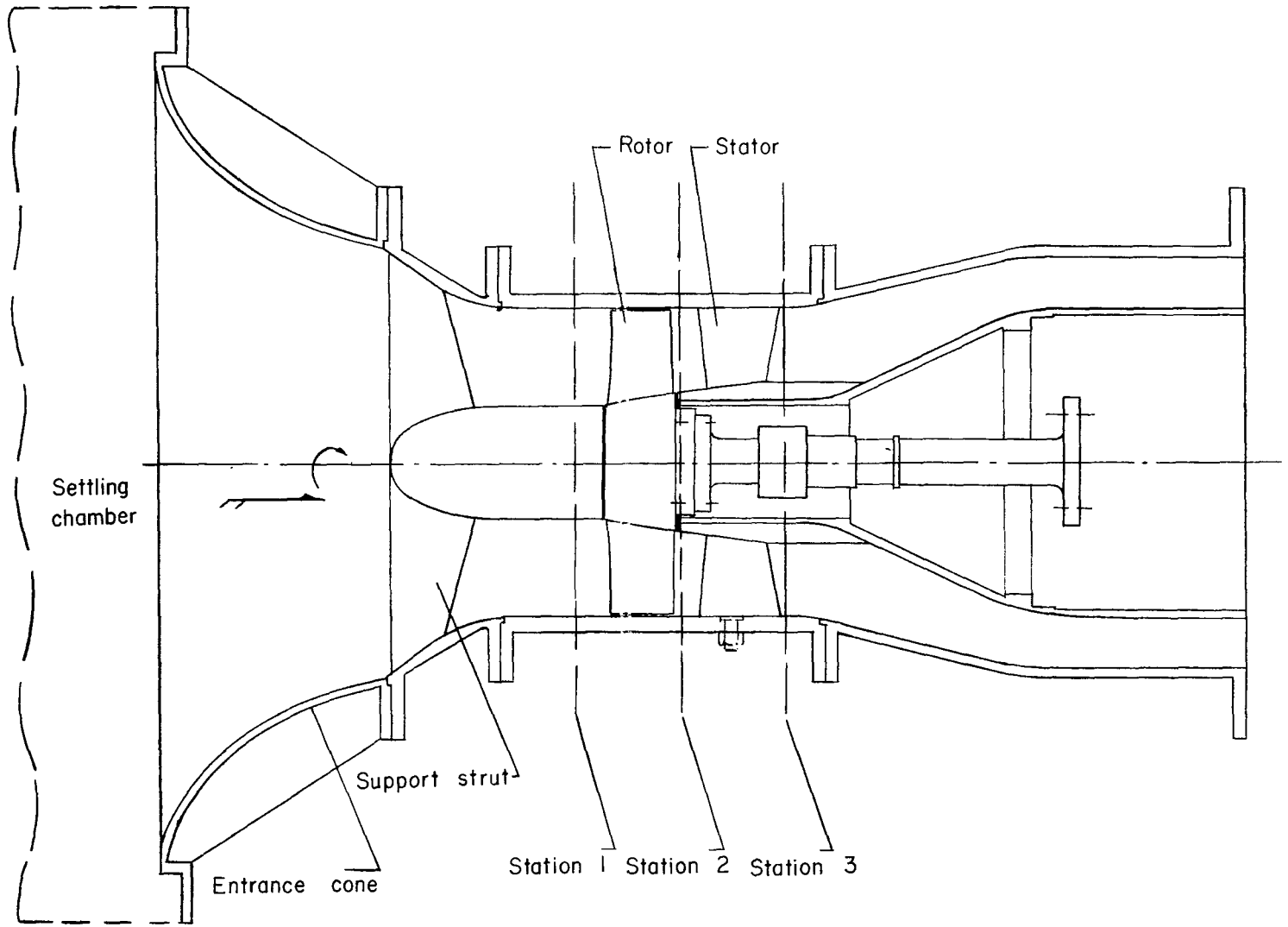

Figure 5.- Schematic diagram of test section.

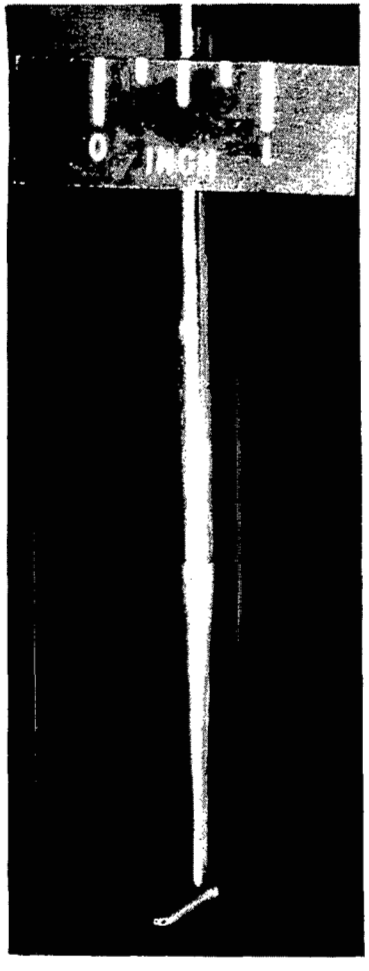

Prism probe

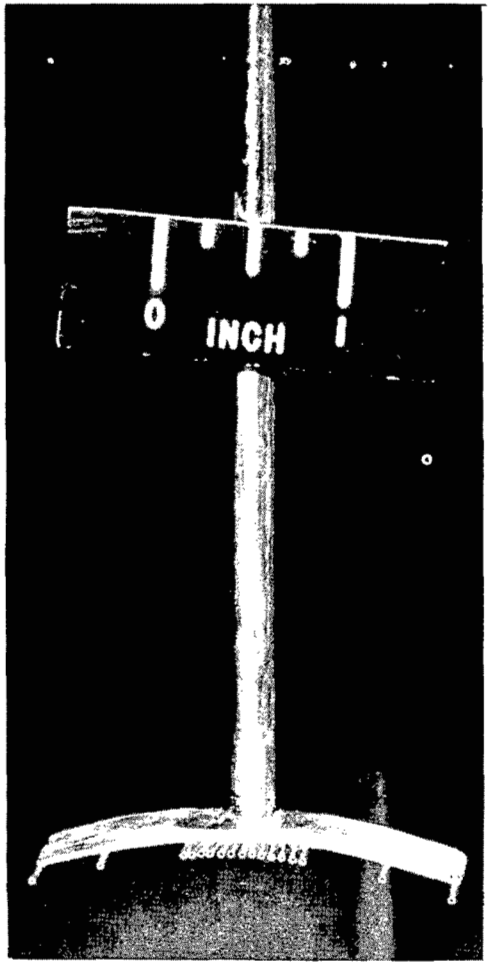

Circumferential total-pressure rake

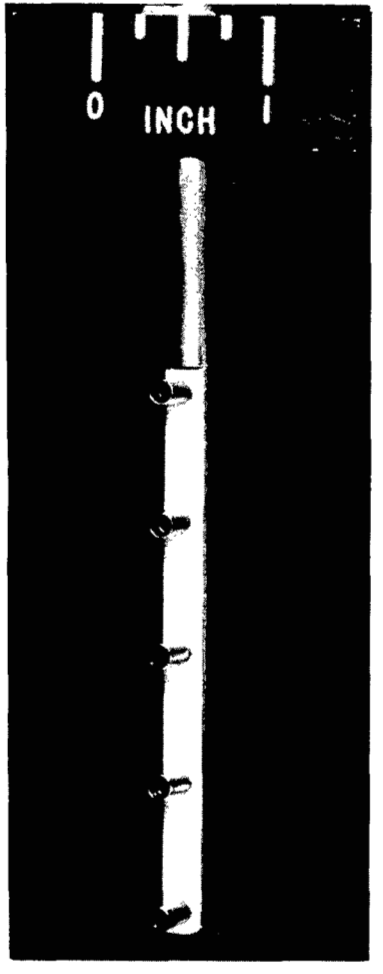

Total-temperature rake

Figure 6.- Photographs of instruments. L-57-4500

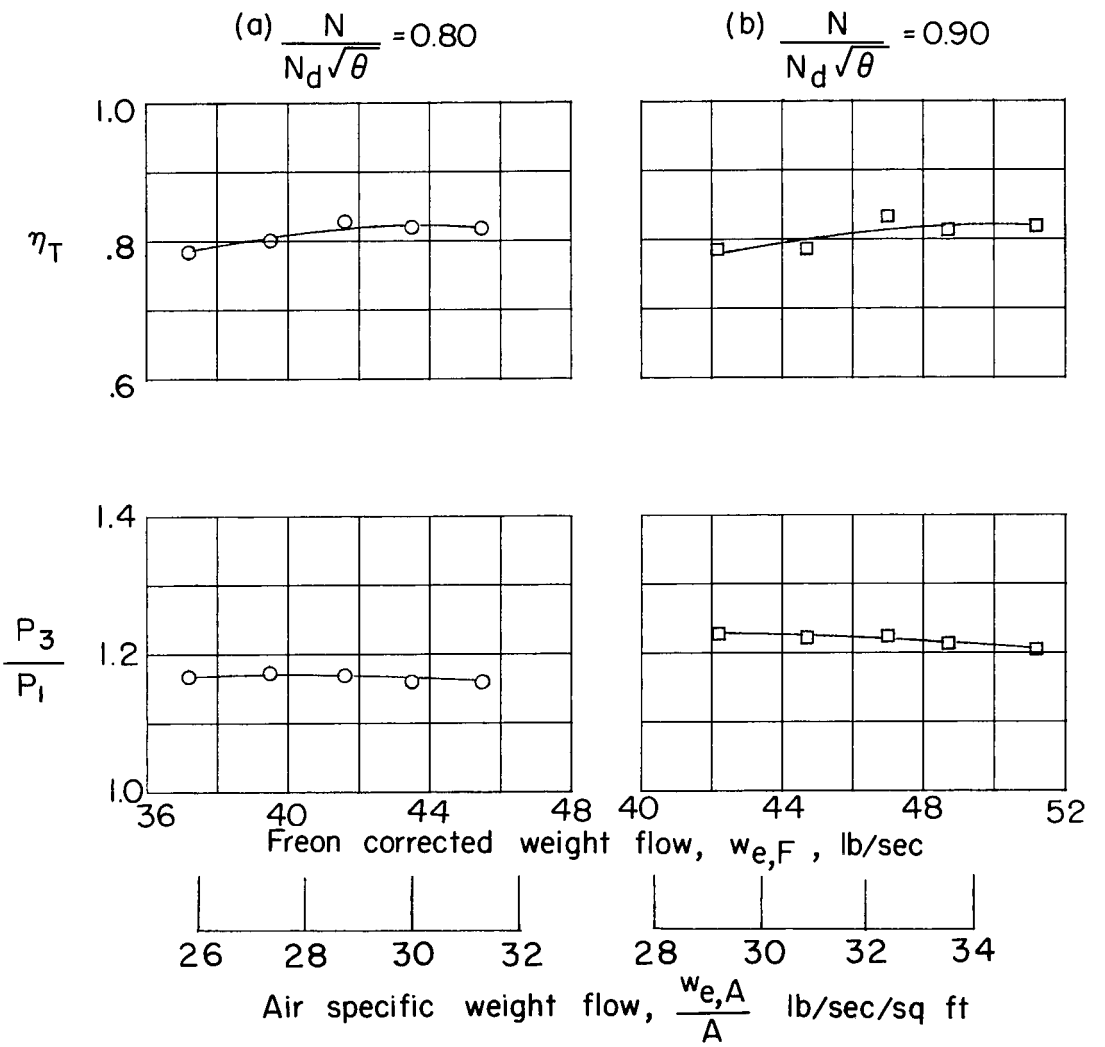

Figure 7.- Mass-averaged overall performance of stage.

[redacted]

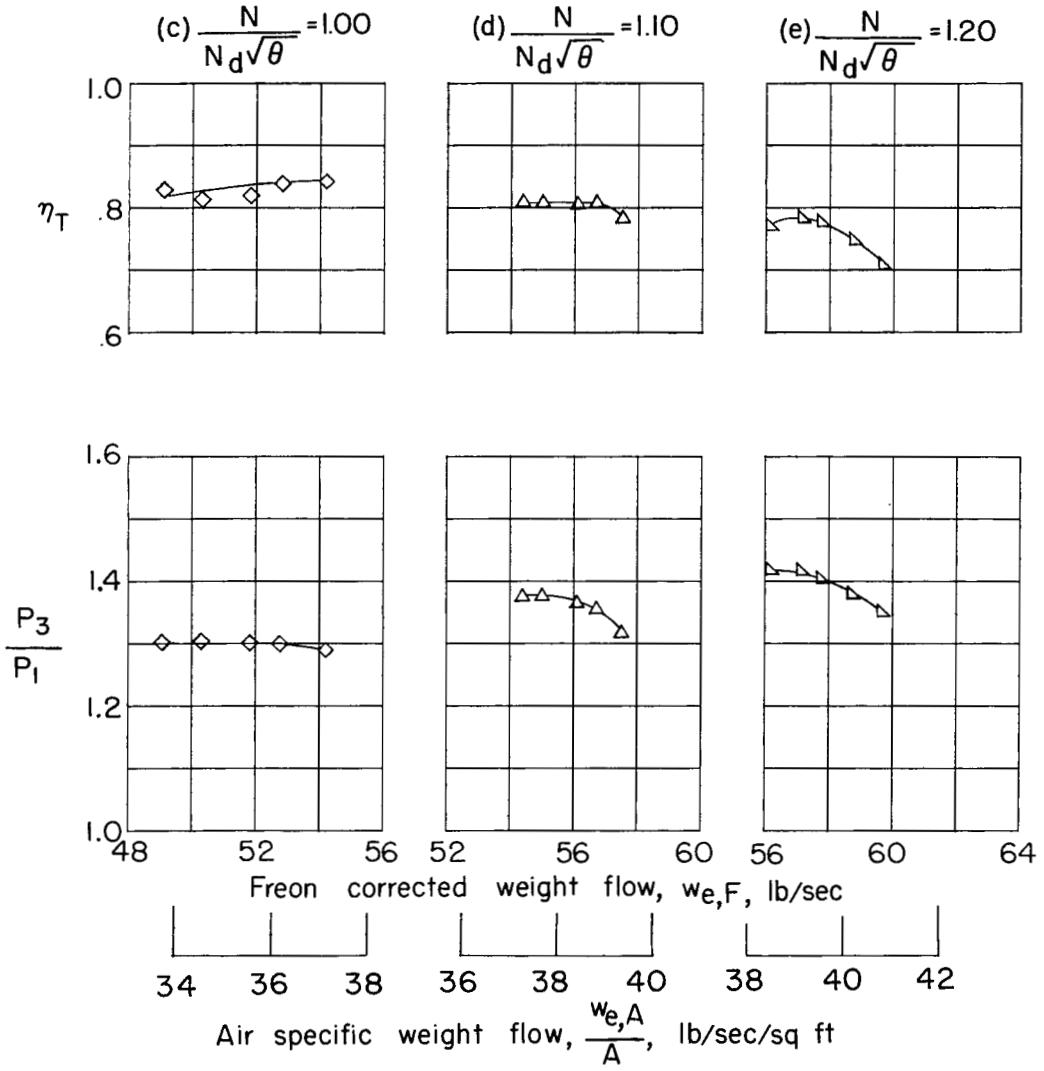

Figure 7.- Concluded.

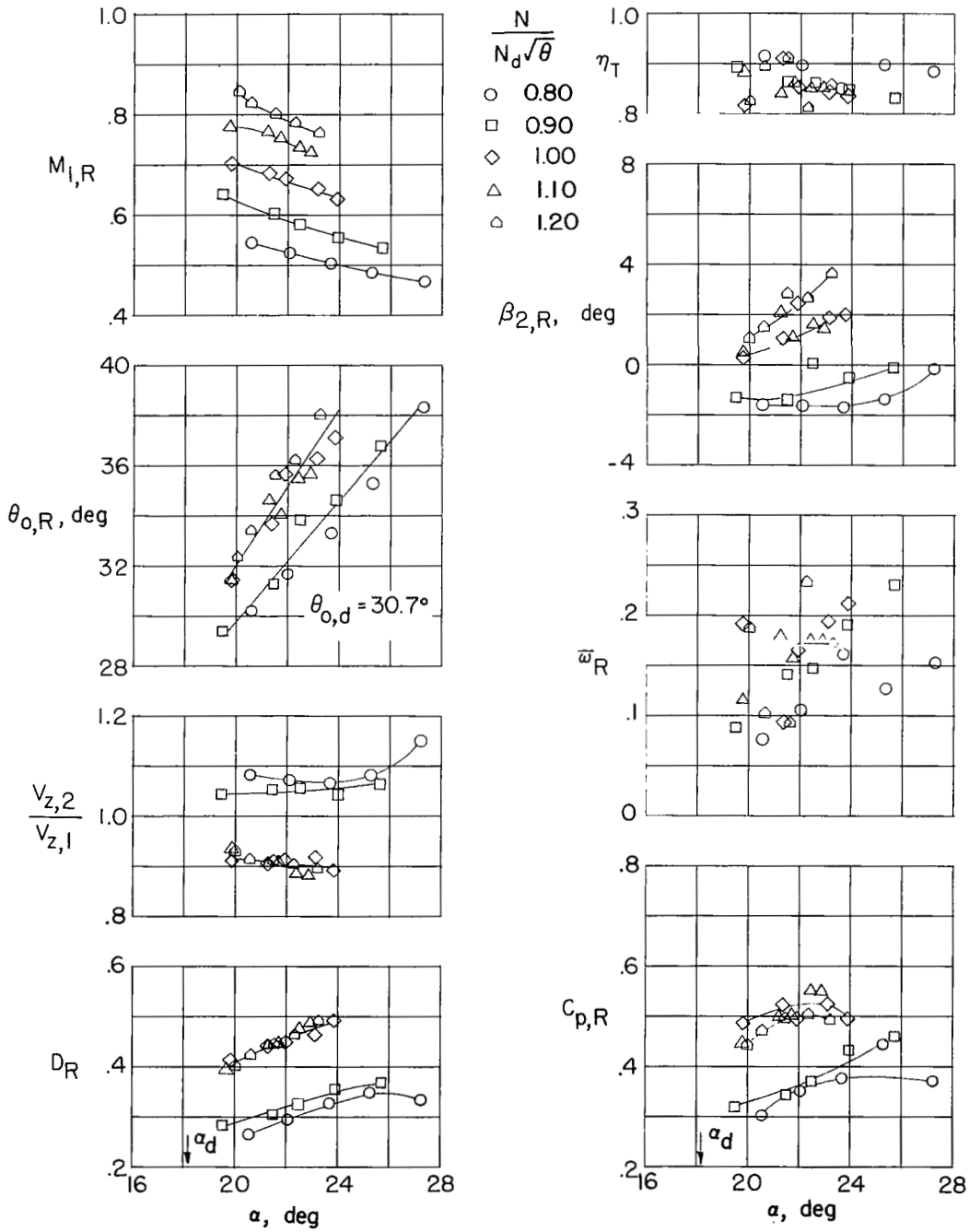

(a) Rotor blade element a; r_1 = 0.204 foot.

Figure 8.- Rotor blade-element performance.

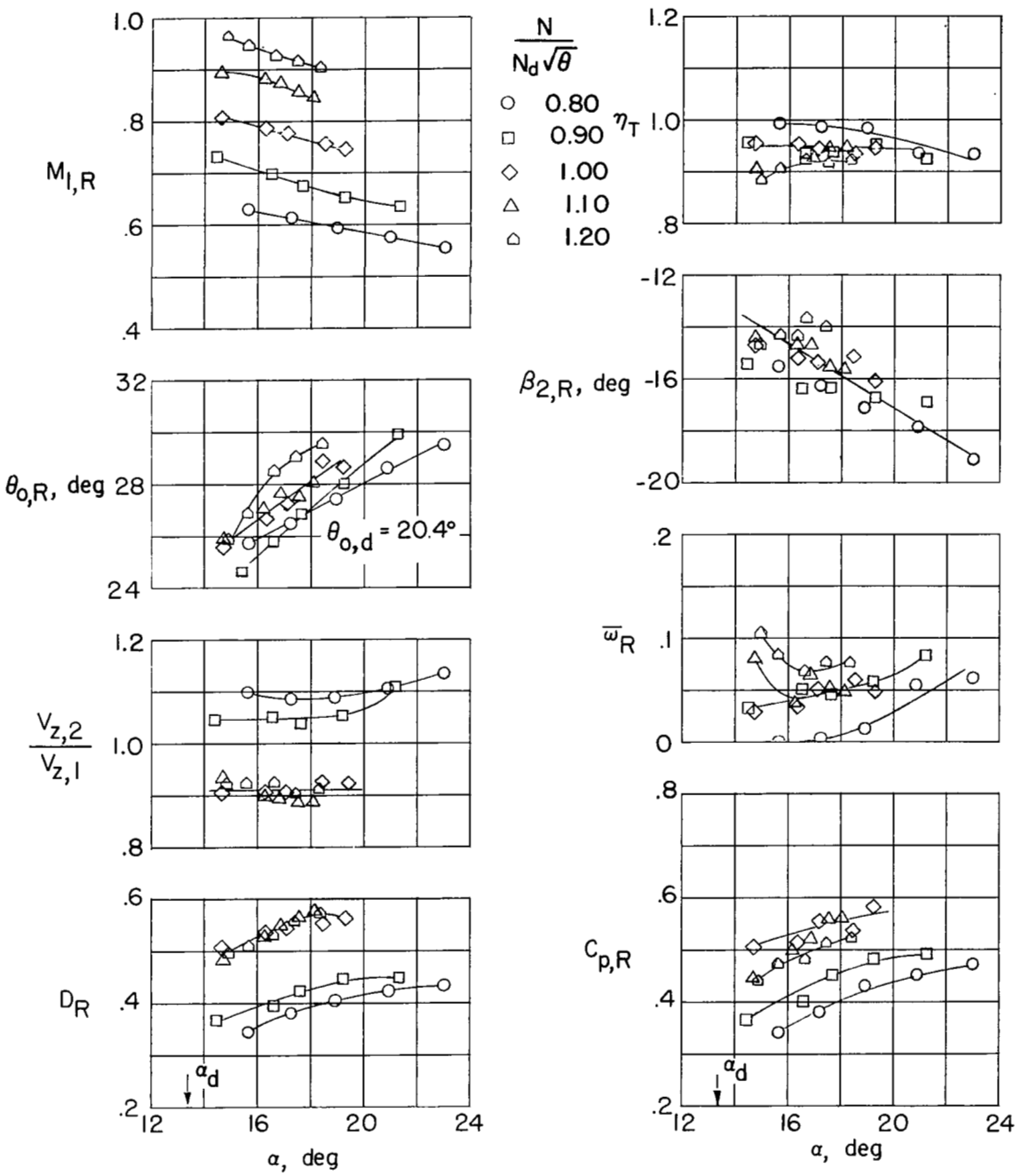

(b) Rotor blade element b; r_1 = 0.292 foot.

Figure 8.- Continued.

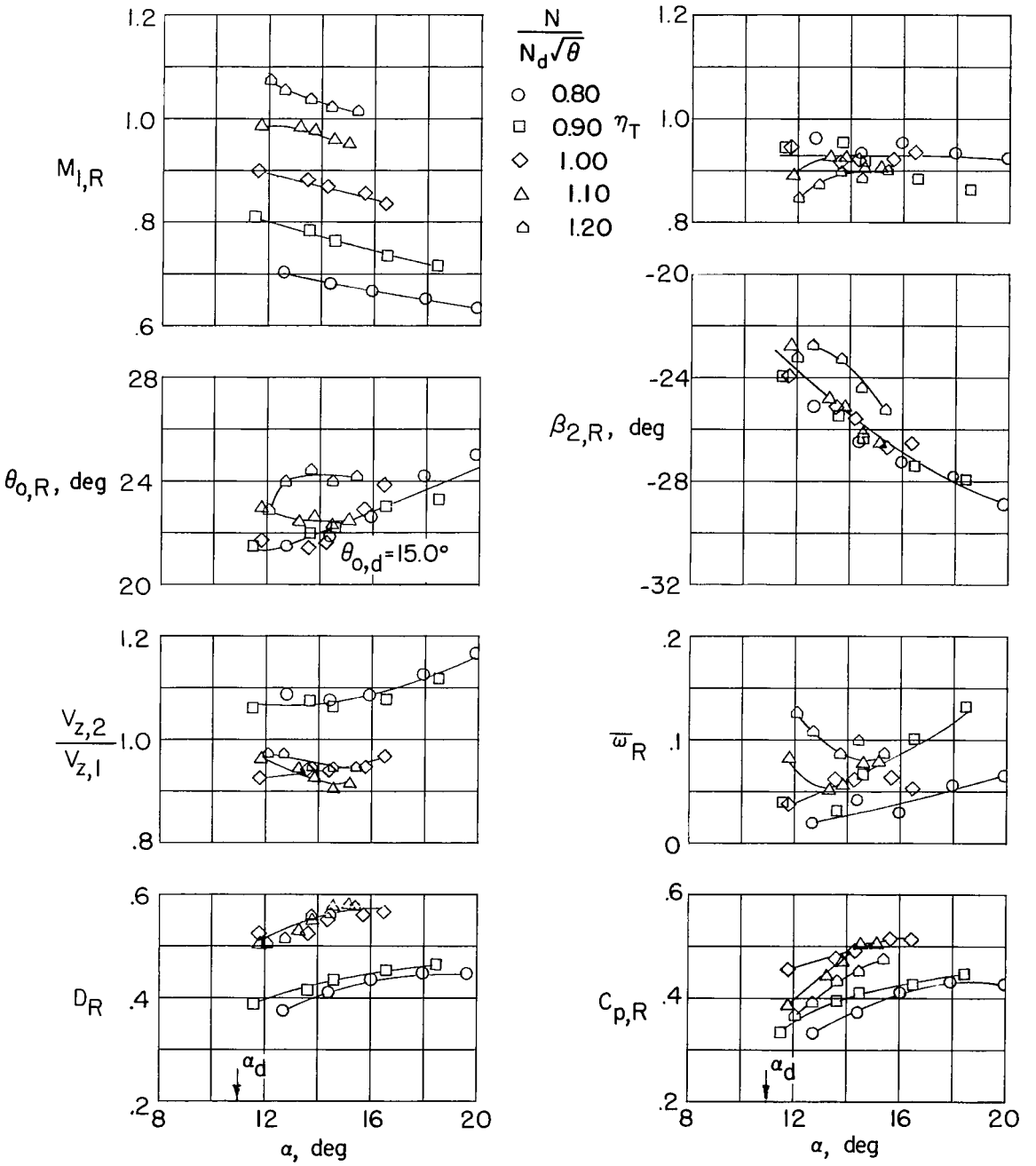

(c) Rotor blade element c; r_1 = 0.360 foot.

Figure 8.- Continued.

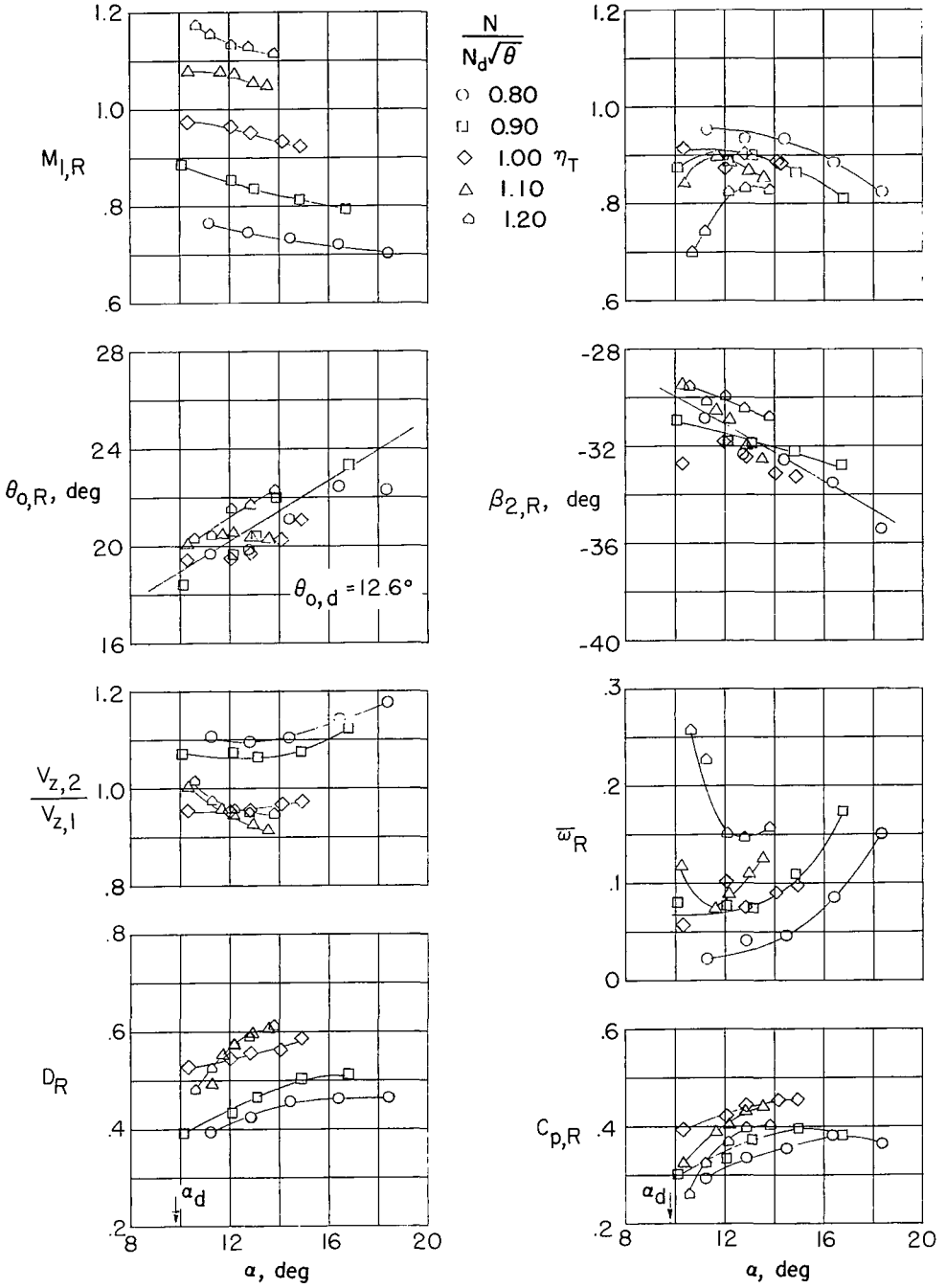

(d) Rotor blade element d; r_1 = 0.416 foot.

Figure 8.- Continued.

[redacted]

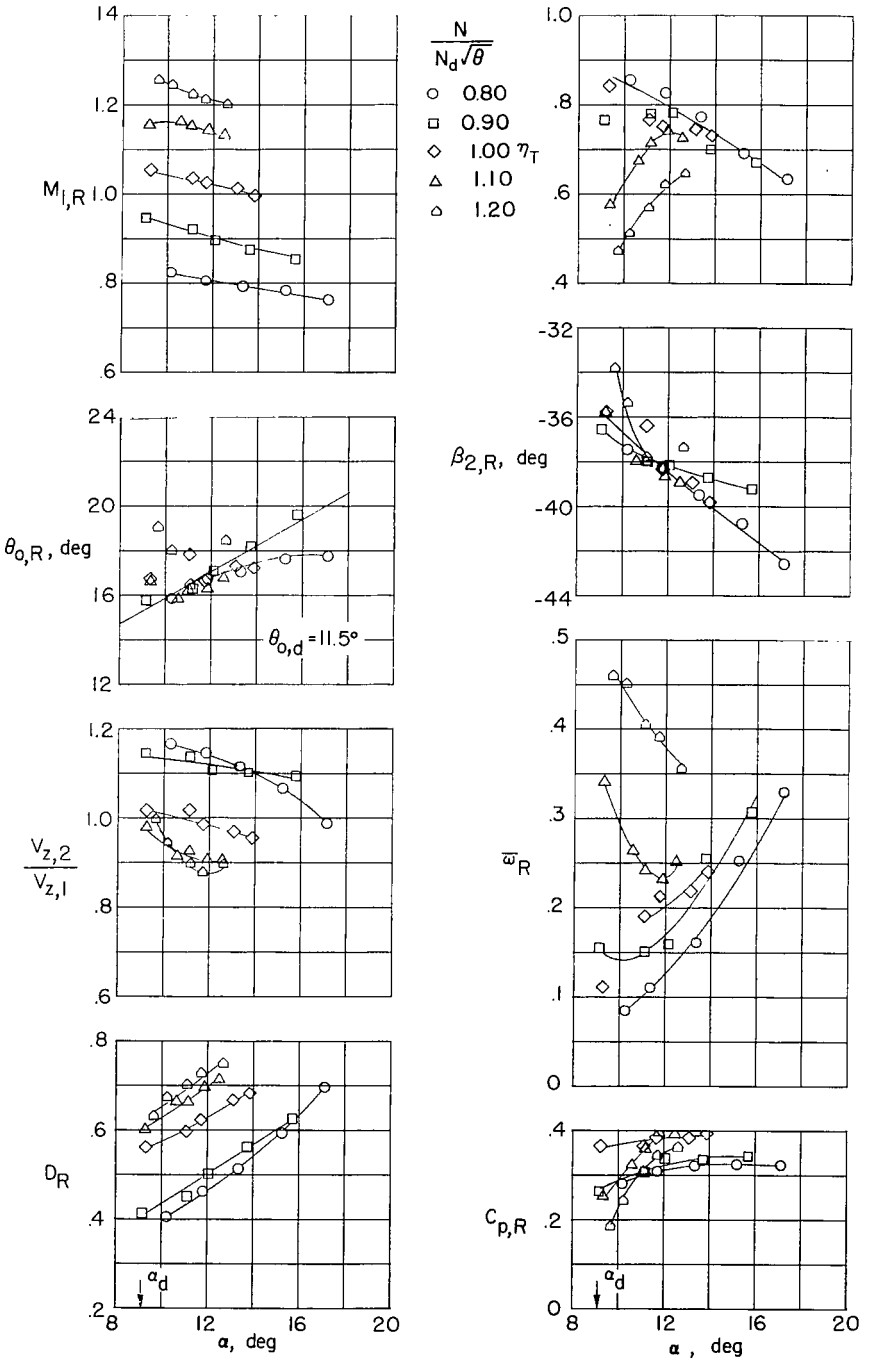

(e) Rotor blade element e; r_1 = 0.466 foot.

Figure 8.- Concluded.

[redacted]

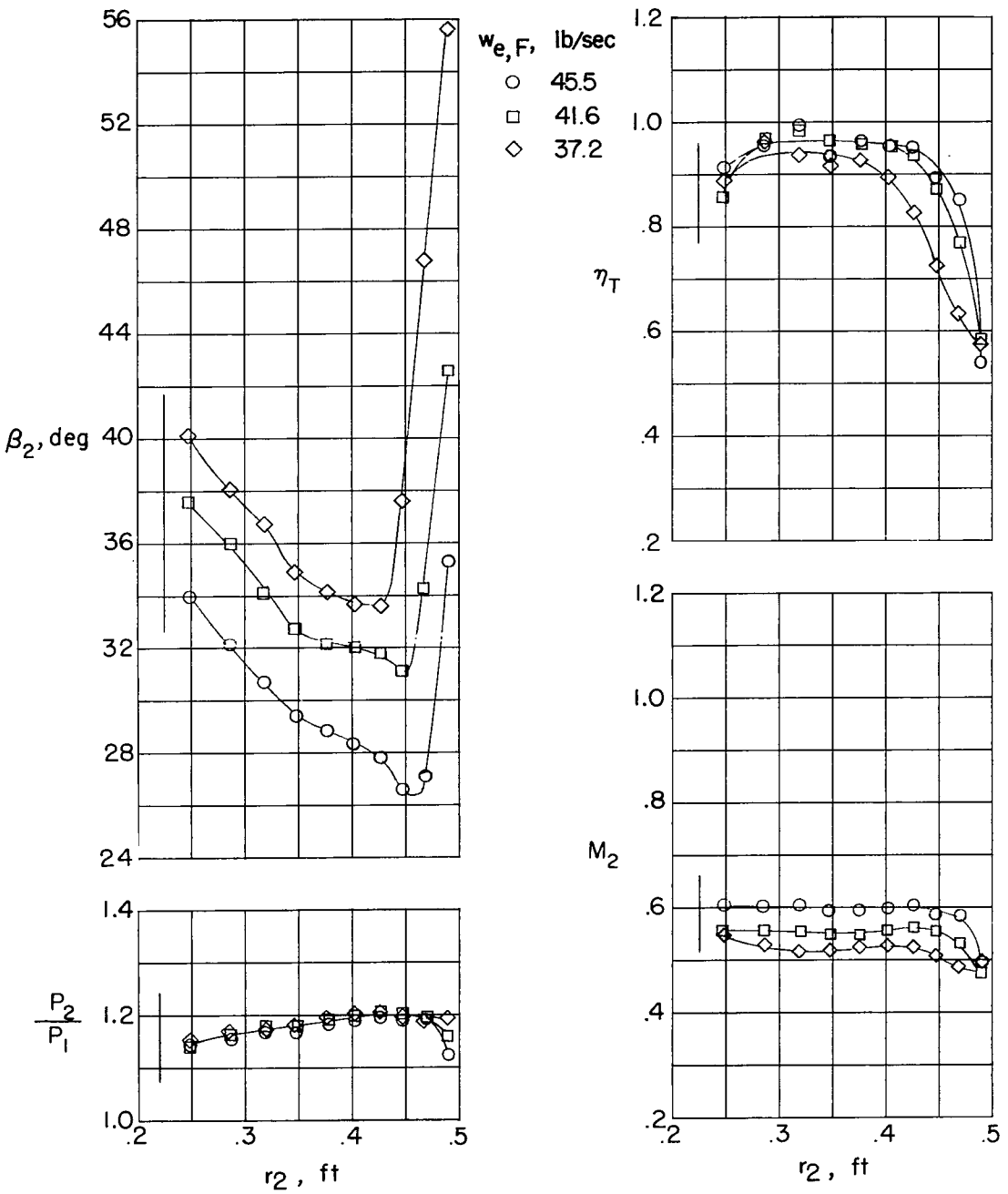

(a) $\frac{N}{N_d\sqrt{\theta}} = 0.80$.

Figure 9.- Radial variation of rotor outlet conditions.

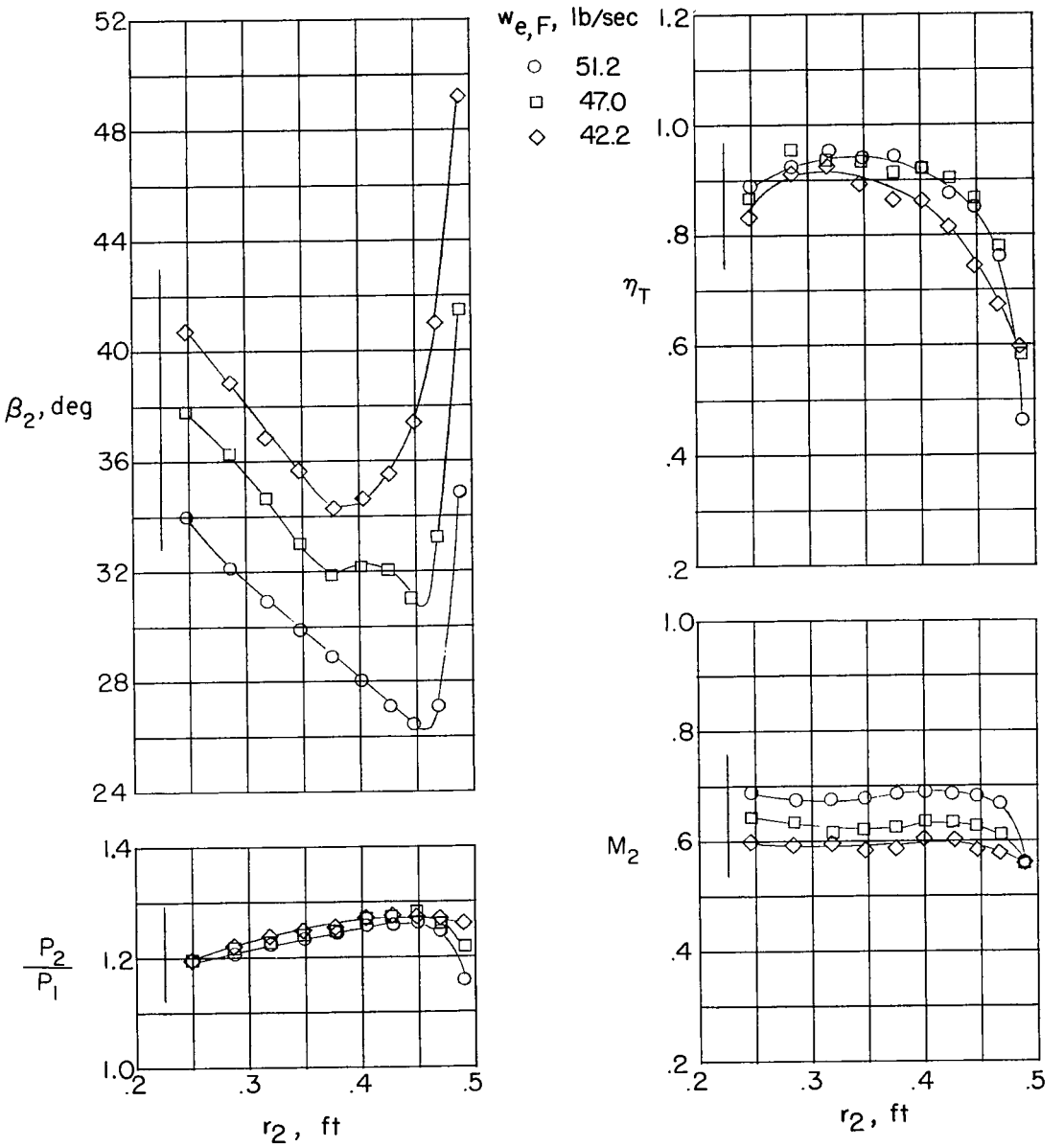

(b) $\frac{N}{N_d\sqrt{\theta}} = 0.90$.

Figure 9.- Continued.

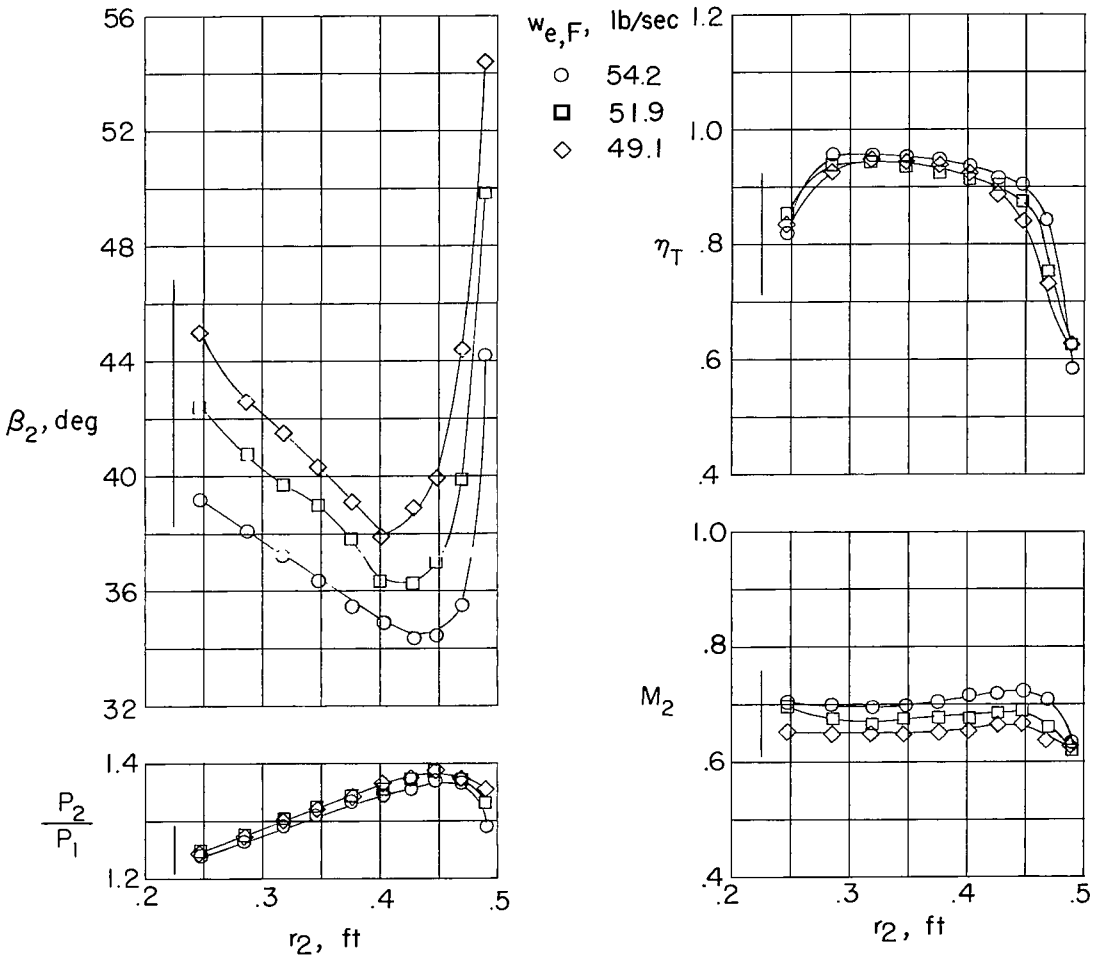

(c) $\frac{N}{N_d\sqrt{\theta}} = 1.00$

Figure 9.- Continued.

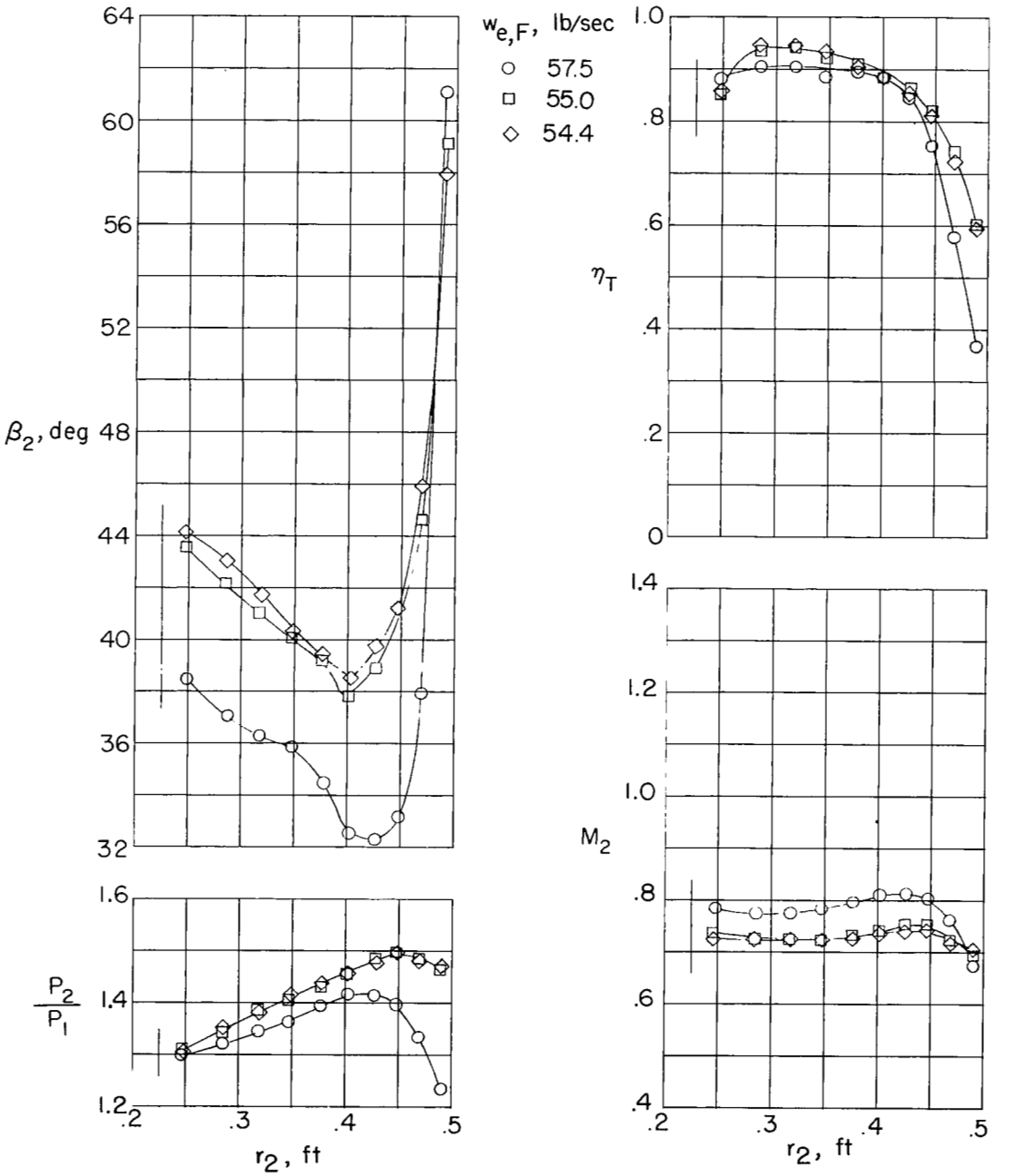

(d) $\frac{N}{N_d\sqrt{\theta}} = 1.10$.

Figure 9.- Continued.

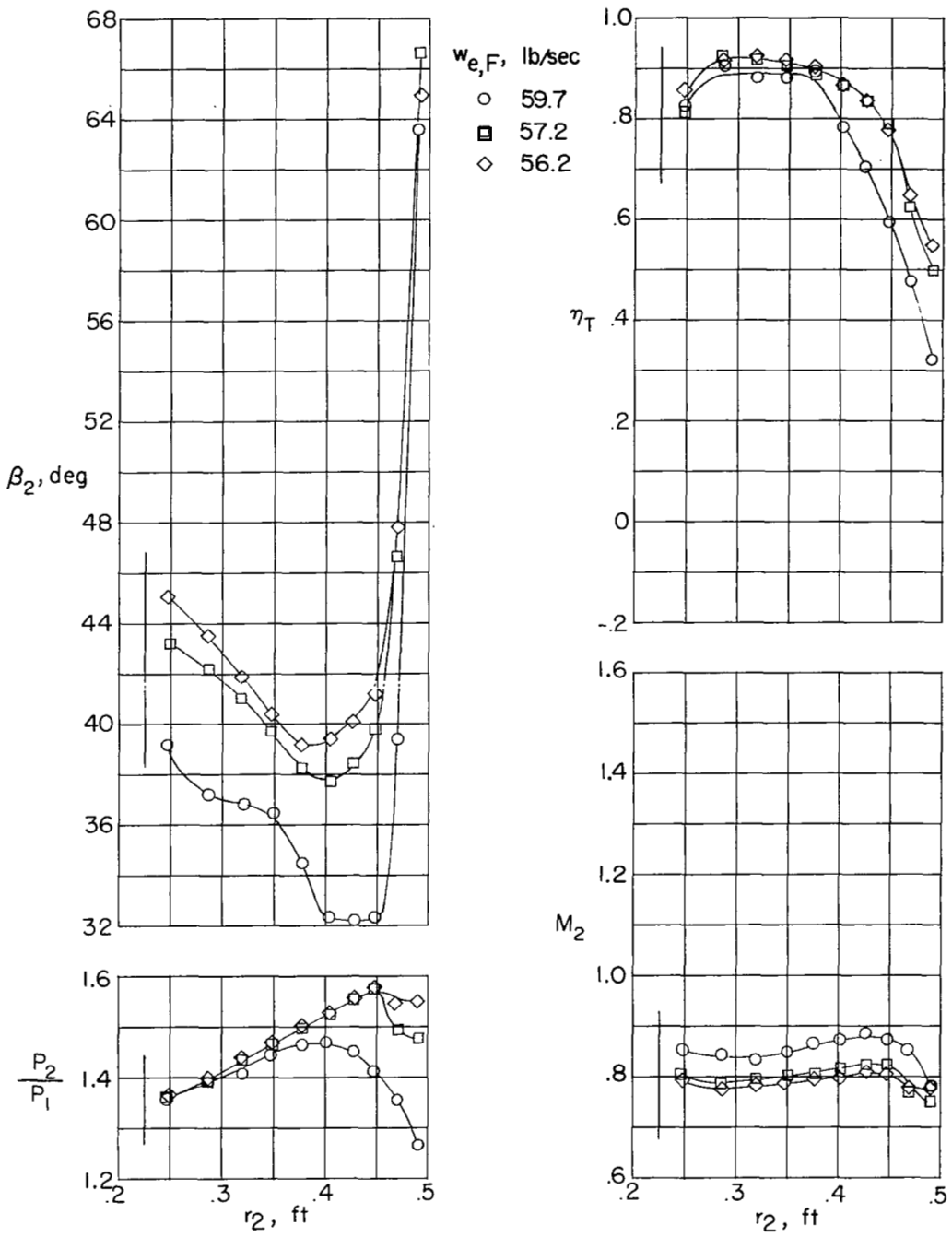

(e) $\frac{N}{N_d\sqrt{\theta}} = 1.20.$

Figure 9.- Concluded.

[redacted]

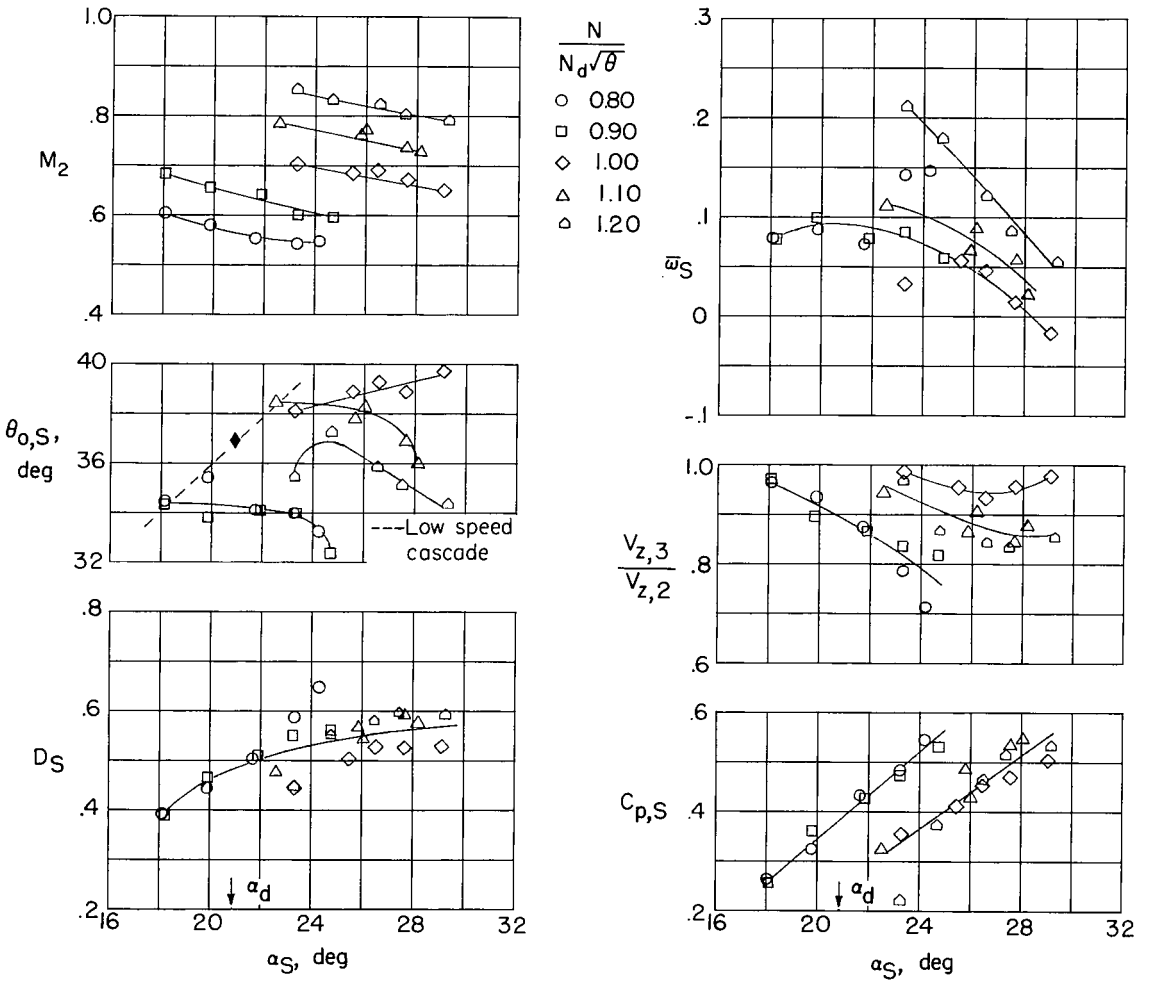

(a) Stator blade element a; r_2 = 0.249 foot.

Figure 10.- Stator blade-element performance.

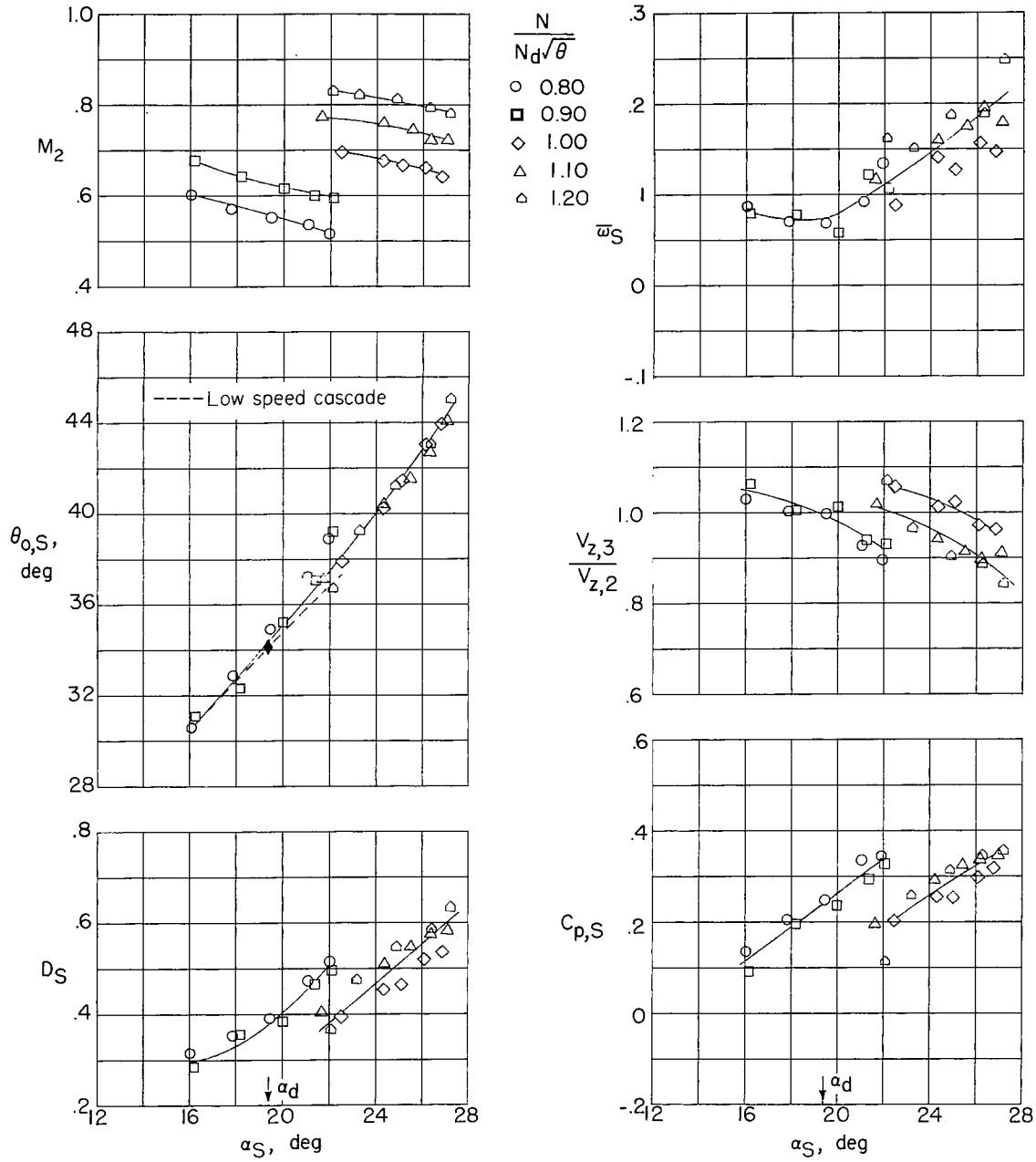

(b) Stator blade element b; r_2 = 0.319 foot.

Figure 10.- Continued.

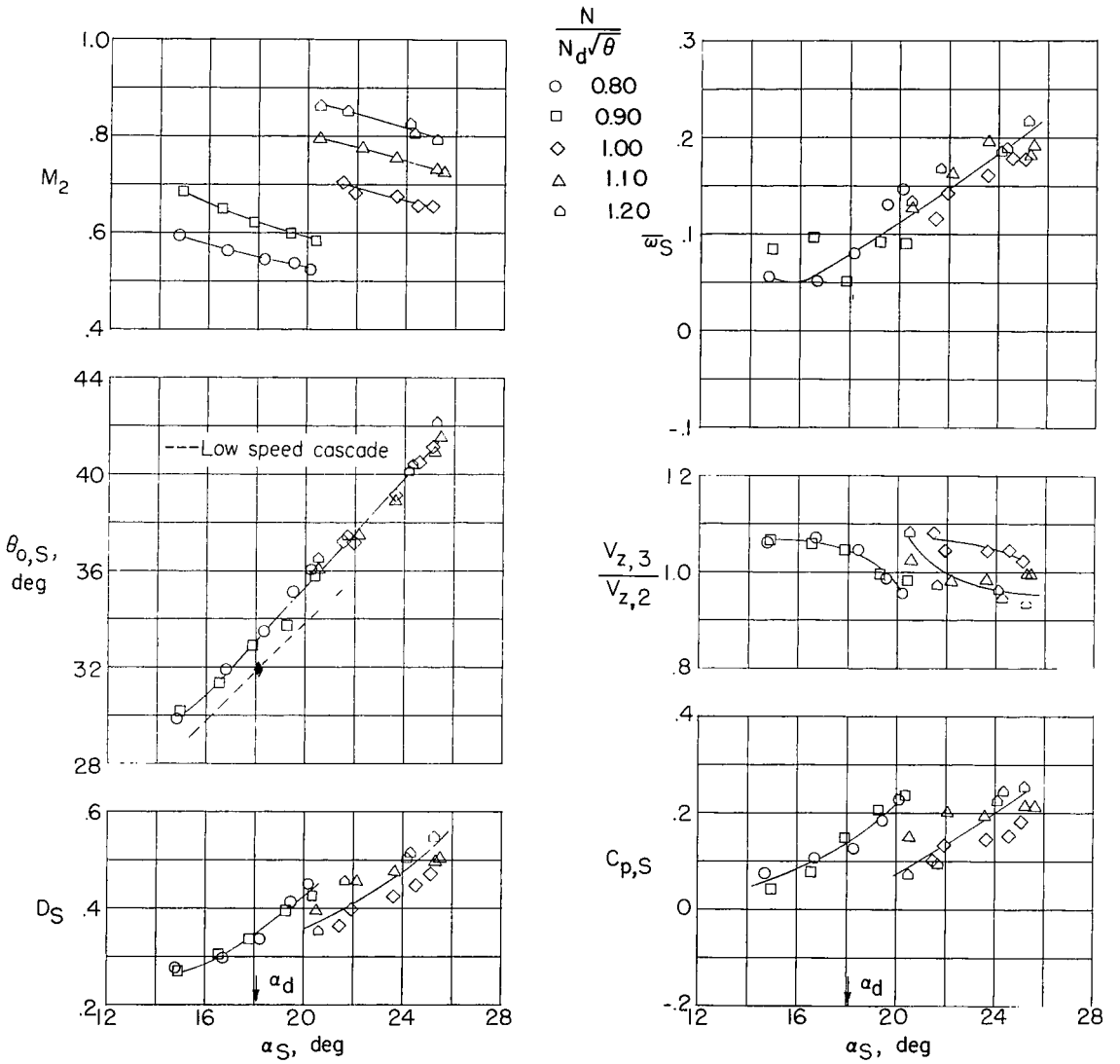

(c) Stator blade element d; r_2 = 0.425 foot.

Figure 10.- Continued.

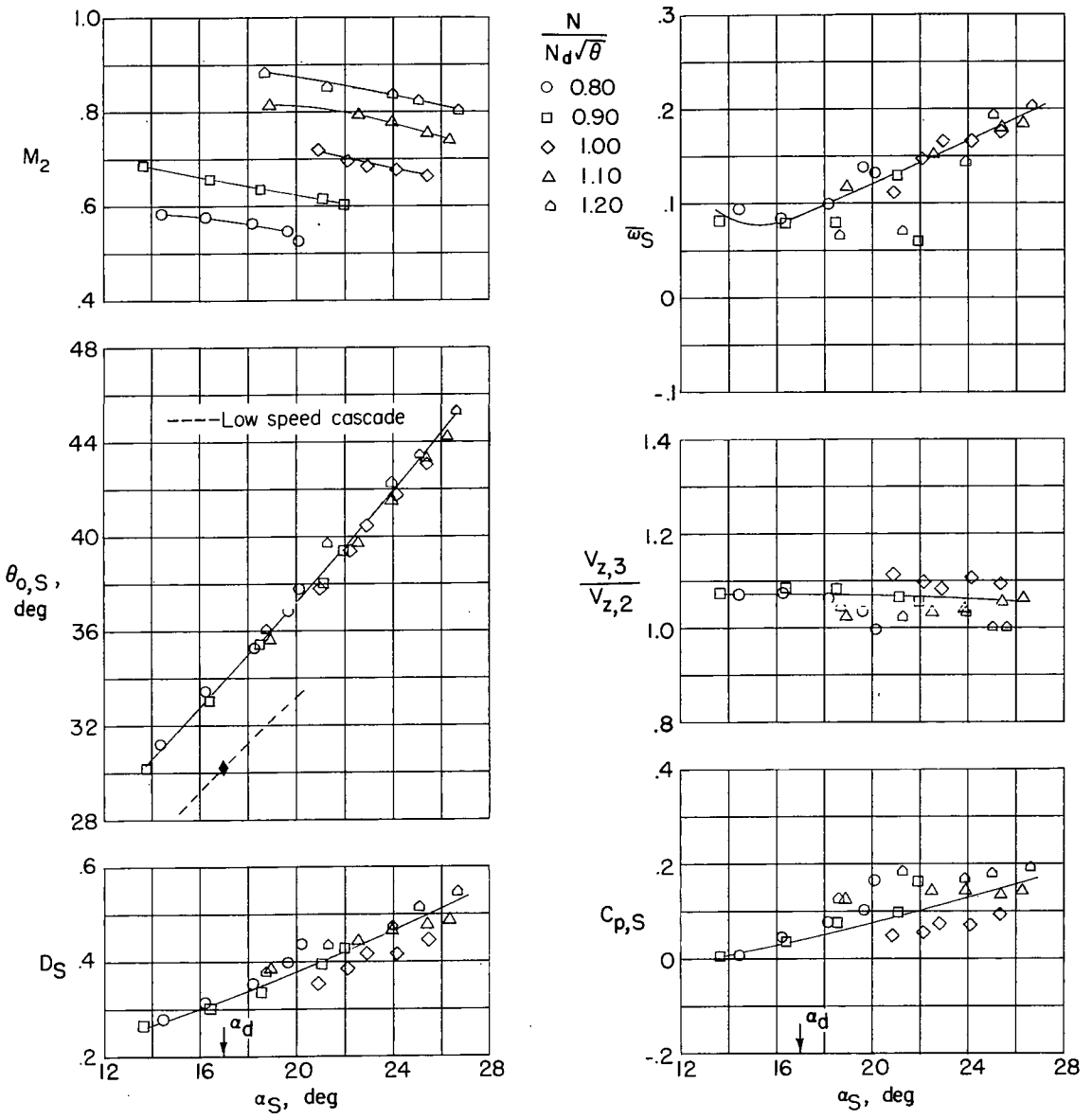

(d) Stator blade element c; r_2 = 0.376 foot.

Figure 10.- Continued.

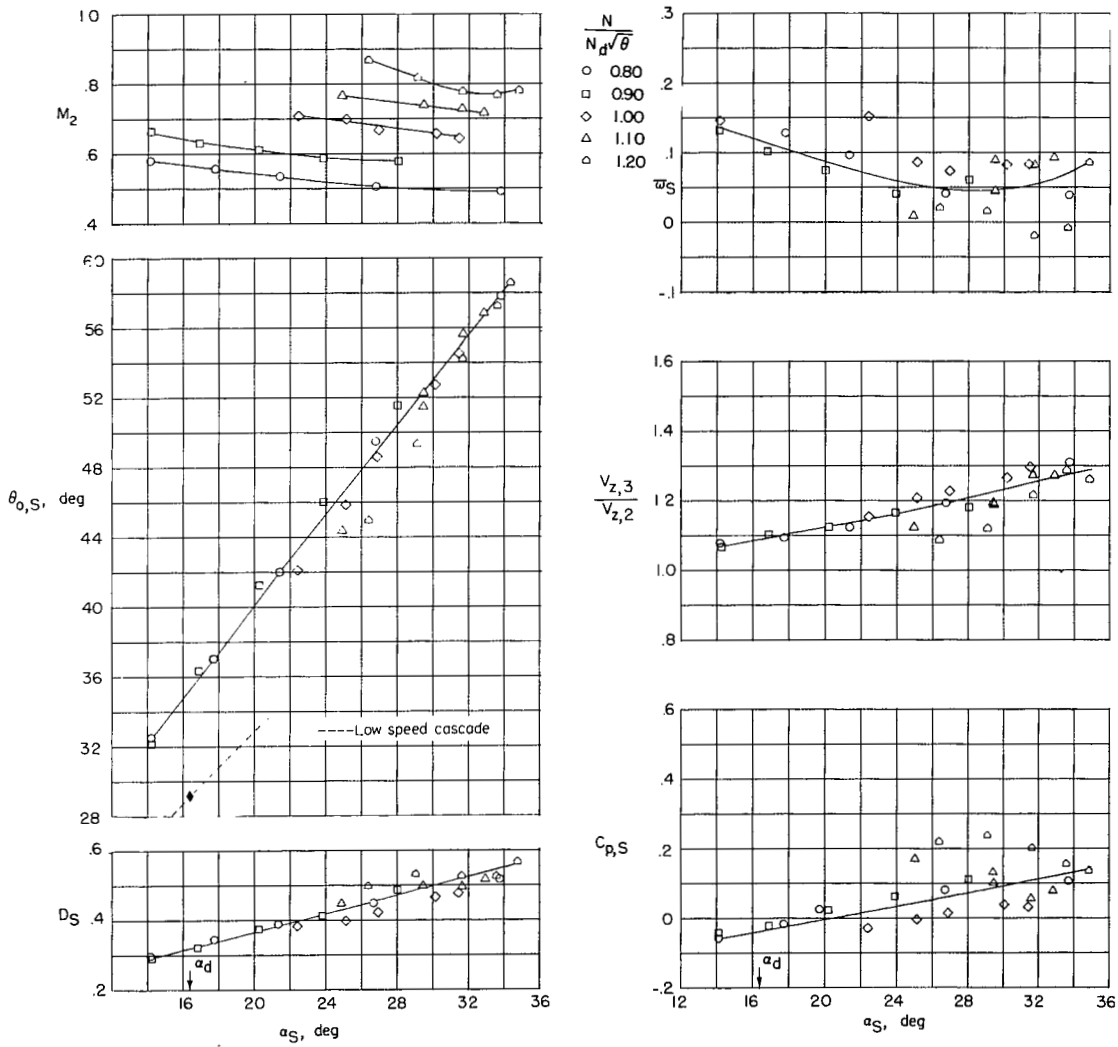

(e) Stator blade element e; r_2 = 0.469 foot.

Figure 10.- Concluded.

[redacted]

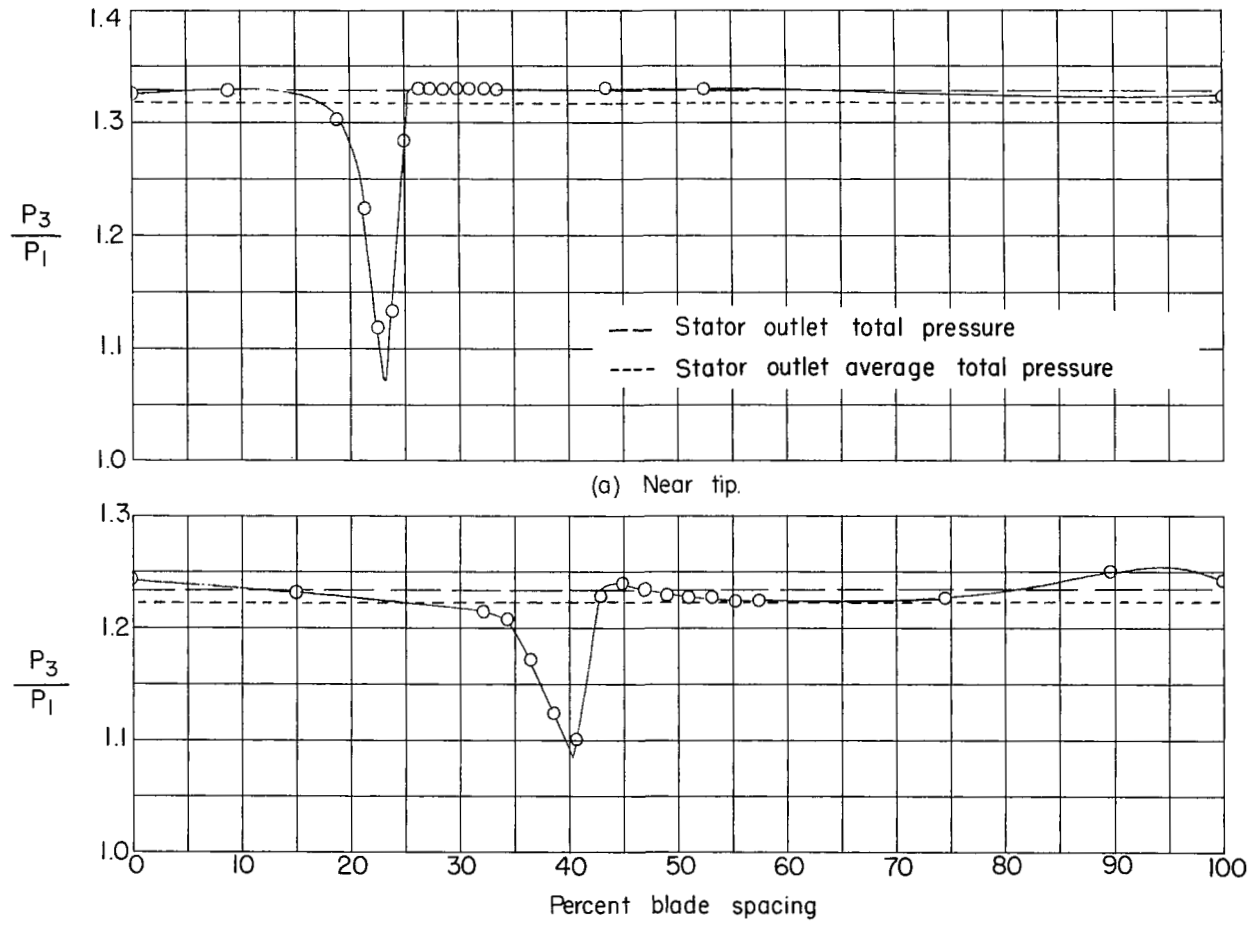

(b) Near hub.

Figure 11.- Typical circumferential variation of total pressure at stator outlet (station 3).

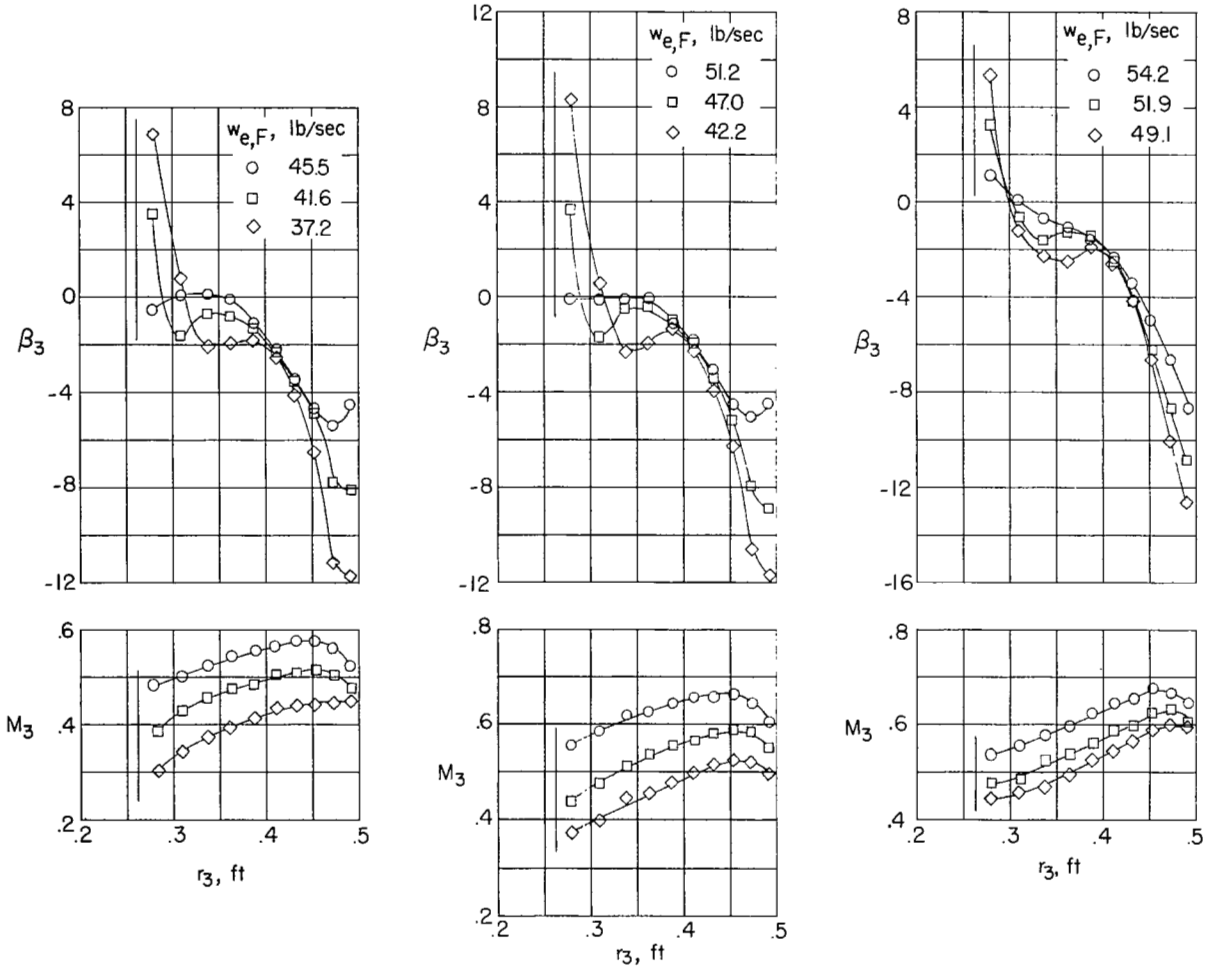

(a) $\frac{N}{N_d\sqrt{\theta}} = 0.80.$ (b) $\frac{N}{N_d\sqrt{\theta}} = 0.90.$ (c) $\frac{N}{N_d\sqrt{\theta}} = 1.00.$

Figure 12.- Radial variation of stator outlet conditions.

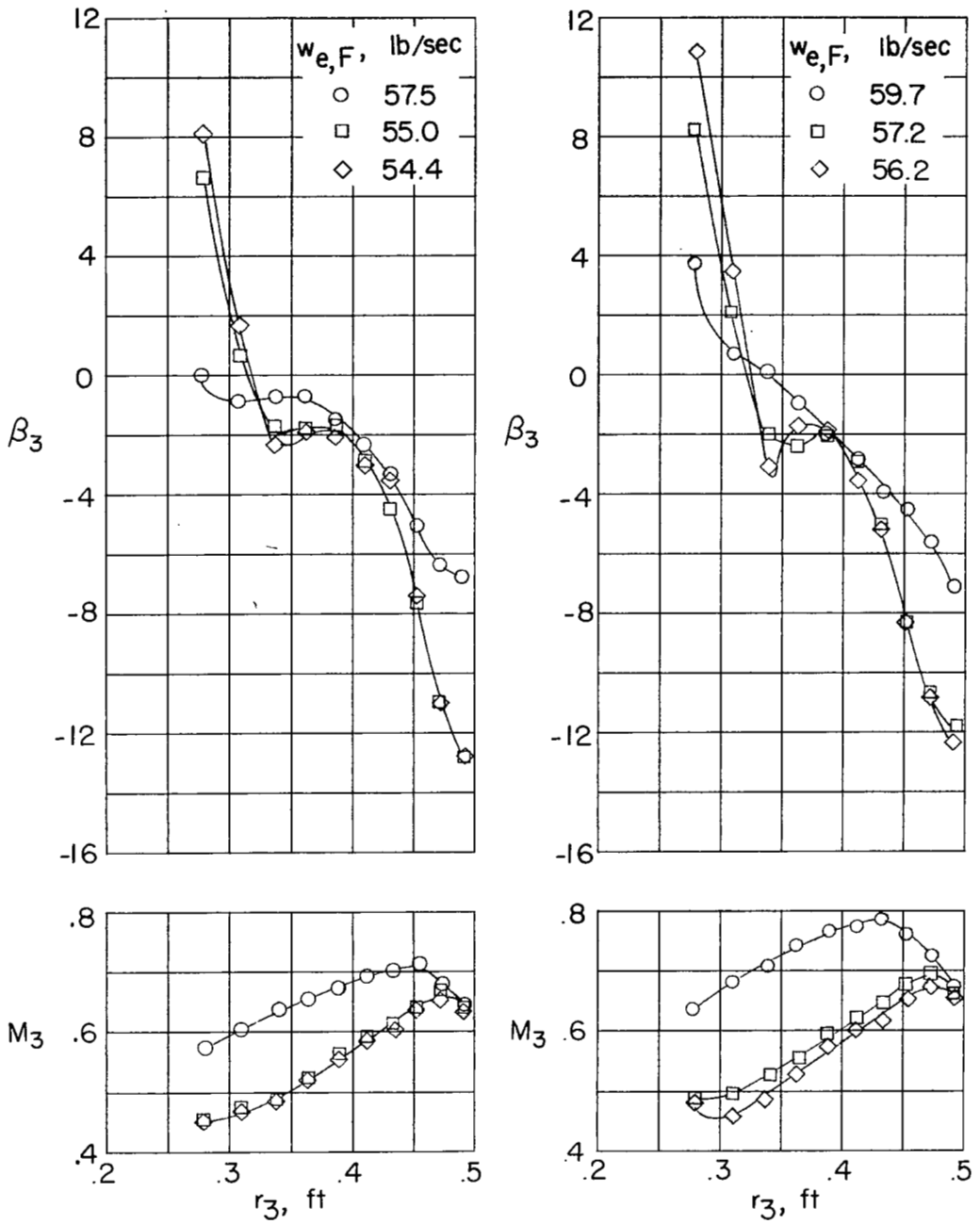

(d) $\frac{N}{N_d\sqrt{\theta}} = 1.10.$

(e) $\frac{N}{N_d\sqrt{\theta}} = 1.20.$

Figure 12.- Concluded.

[redacted]

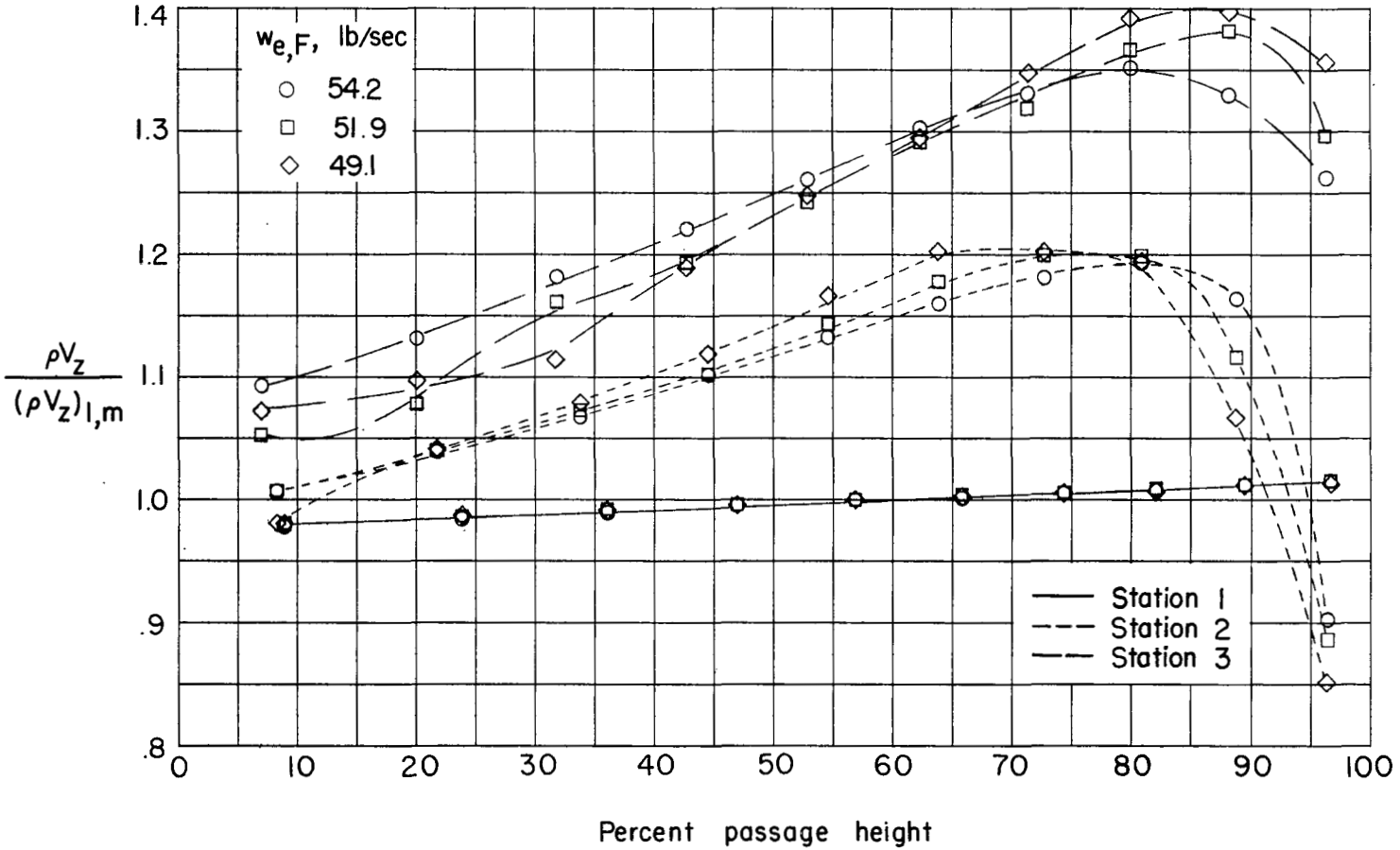

Figure 13.- Radial distribution of weight flow at design speed.